FREQUENCY STABILITY OF A HELIUM NEON LASER SYSTEM WITH EXTERNAL CAVITY CONTROL

by

Robert Lee Kurtz

Thesis submitted to the Graduate Faculty of the

Virginia Polytechnic Institute

in partial fulfillment for the degree of

MASTER OF SCIENCE

in

Physics

APPROVED: _____

Chairman, Dr. H. Y. Loh

_____

Dr. J. A. Jacobs

_____

Dr. R. L. Bowden

_____

Dr. T. E. Gilmer

June 1968

Blacksburg, Virginia

TABLE OF CONTENTS

ACKNOWLEDGMENTS

The author would like to express his appreciation to his advisor, , of the Virginia Polytechnic Institute for his sustained interest, guidance and cooperation. Appreciation is also expressed to of the University of Alabama for his helpful discussions and assistance with the computer program.

The author wishes to thank and for their diligent efforts in the typing of this manuscript.

The author offers an expression of gratitude to his wife, , for her help and encouragement during the preparation of this manuscript.

LIST OF TABLES

LIST OF FIGURES

LIST OF FIGURES (continued)

I. INTRODUCTION

Many applications of gas lasers depend upon the extremely high spectral purity of their output signals. To exploit or fully utilize this remarkable spectral purity requires a high degree of frequency stabilization and laser mode control. An example of the use of this frequency stabilization in a laser system is as the local oscillator in a communication system. In such a system, frequency drift in the laser would require a broadened bandwidth in the receiving system, with a concomitant increase in noise level. Other examples are the use of a laser for Doppler velocity measurements, or in a device for measuring angular rate by the Michelson-Gale effect, etc. In uses of this type, any drift in the laser frequency would result in direct errors in the measurement undertaken.

Some evident causes of frequency instability in gas lasers are as follows:

1. Temperature Changes

   a. Those which lead to a physical change in the separation of the mirrors because of the thermal expansion of the connecting parts of the resonant cavity.

   b. Those which cause a change in the optical pathlength between fixed mirror spacing due to a change in the index of refraction.

2. Resonant vibration of the structure and acoustical disturbances.

On a contract let by the National Aeronautics and Space Administration (NASA) of Marshall Space Flight Center, Alabama, the Perkin-Elmer Corporation of Norwalk, Connecticut developed a helium neon laser system,

frequency stabilized to the resonant frequency of a passive external resonator. This is the optical analog of the use of an external cavity to control the frequency of a microwave oscillator.

In order to obtain a knowledge of the degree of frequency stability currently possible, an investigation of this system was undertaken. The long and short term frequency stability was experimentally measured for both the open and closed loop cases. The resulting data were analyzed to produce state-of-the-art results for frequency stabilization of helium neon gas lasers.

II. REVIEW OF LITERATURE

A comprehensive computer search of the literature was undertaken through the facilities of Marshall Space Flight Center (MSFC), Marshall Space Flight Center, Alabama. A considerable amount of literature was found on laser stabilization at 6328Å. The most pertinent of these have been included in the Bibliography. Most of these references deal directly with some method of frequency stabilization of 6328Å helium neon lasers both dc and RF excited.

The paper most necessary as preparation for the present discussion is "Laser Wavelength Stabilization with a Passive Interferometer" (8). This paper resulted from an investigation by Dr. Lipsett and Mr. Lee of the Perkin-Elmer Corporation, in prelude to the development of the system subsequently investigated and evaluated by this author.

Their approach was to develop a control system for stabilizing the output wavelength of a laser by reference to an external passive optical element. This element consisted of two spherical mirrors, forming an off axis resonator which, when broadly illuminated by a laser beam, functioned as a wavelength-sensitive discriminator. The stabilization control loop was closed by using a signal from this discriminator to tune the laser by moving one of its mirrors with a piezoelectric transducer. The developed error signal was a function of the changes in wavelength of the incident laser beam and was derived from the discriminator without deliberate frequency or amplitude modulation of the laser. The optical arrangement returned no light in the direction of the source and thereby avoided any wavelength pulling due to spurious reflections.

In their investigation, Dr. Lipsett and Mr. Lee had two independent helium neon lasers operating at 6328Å and stabilized against a common reference interferometer. The system investigated by this author, however, had two independent laser systems, each with its own separate passive interferometer. The passive interferometers of systems one and two possessed the proper geometry to produce a beat signal between them of 150 megacycles.

A review of the different methods of frequency stabilization is presented as a means of directing the reader's attention to the various methods of frequency stabilization currently employed. The methods are listed separately, followed by their reference in the Bibliography. Many references employed more than one of these stabilization schemes, but a reference is given only if that reference placed particular emphasis on that particular scheme.

The methods of frequency stabilization currently employed are:

1. Temperature control; (1, 3, 8, 9).
2. Mechanical stability of resonant cavity; (1, 3, 4, 16, 17).
3. Single mode operation; (1, 3, 4, 5, 7, 8, 9, 12, 16, 17, 19).
4. Control of gas excitation; (4, 7).
5. Double mode operation producing a self beat frequency which is phase locked to a frequency standard; (6).
6. External off axis passive interferometer producing an optical discriminant; (8).
7. Manual control of resonant cavity length, using a piezoelectric crystal; (9).
8. Phase locked scheme; (10).

9. Use of axial magnetic field around laser with internal mirrors to produce an error signal to be applied to correct cavity length; (11, 19, 21).

10. A method of gain dither; (12).

11. Modulation of length of resonant cavity; (14, 15).

12. Acoustic isolation; (3).

13. Use of external Fabry-Perot "active" filter; "active" in that the mirror spacing of this external filter is automatically controlled; (16).

14. Use of three mirror interferometers as one of the end mirrors of the resonant cavity. Two of the three mirrors in this interferometer were outside of the resonant cavity, so one of these was automatically controlled so that the interferometer arm was variable and this varied the reflectivity of the resonant cavity mirror; (16, 17).

15. Some form of automatic feedback system; (6, 8, 10, 11, 14, 15, 16, 17, 19, 21).

The system investigated by this author used a combination of several of the above mentioned methods, i.e., methods 1, 2, 3, 4, 6, 12, and 15.

Reference (20) is singled out as a review of current stabilization methods in its own right. Attention is also called to method 14, which that author describes as a means of correcting for slow thermal drifts, present in all lasers.

III. DESCRIPTION OF FREQUENCY STABLE LASER SYSTEM

A. Laser Housing and Electro-optic Circuit

Figure 1 shows the inside of one of the two system housings*. Each system housing contains the following major components: A single mode He-Ne laser cavity, (located between numbers 10 and 1 of the figure); a resonant reference cavity (number 4 of figure); an optical train for generating the frequency error signal (numbers 5 through 8); various auxiliary optical components, and the two stage proportional temperature controller. The 6328Å light from the laser cavity is incident on a beam splitter (1) which passes 50% of the incident radiation and reflects the rest of the radiation through an aluminum tube (2) to a mirror (3). This light reflected from the mirror illuminates the off axis resonator cavity (4). This radiation may emerge from the cavity only for frequency near resonance, and then in a direction dependent on the frequency of the illuminating light. The output beam from the cavity passes through the split polarization plate and quarter wave plate combination (5) then finally through the modulator and tandem polarizer (6) where it is reflected again by a mirror (7) onto the face of a photomultiplier tube (8). The output of this phototube with sufficient information to develop a discriminant is fed into the servo system control loop in the electronic module, external to the housing. The error signal from the servo system is fed back to a piezoelectric transducer which is capable of minute

---

*Final Report 8369, by Messers. Lee and Skolnik, was quite helpful in this description of the system and its components.

lengthening or shortening of the Fabry-Perot Laser Cavity, and thereby lowering or raising the output frequency of the laser radiation which is incident on beam splitter number 1. Also shown in the photograph (figure 1) are the two thermistor bridges with preamplifiers (9); the six outer case heaters (10); the 100 kHz pusher filter (11) and the vacuum pump connection tube (12) used for the evacuation of the off axis resonant cavity.

Figure 2 is a more candid presentation of the components. It is a schematic of the components and the respective orientations inclusive of the external servo system employed between the photomultiplier output and the laser cavity. This is the schematic of one, of two essentially identical systems, each of whose outputs (shown at top of the figure) were optically combined to produce a beat frequency.

B. Component Description

1. Laser

The resonator of the helium neon laser has a 13.5 cm mirror spacing and two 120 cm radius of curvature mirrors. This geometry restricts the laser oscillation to the fundamental transverse mode (TEM_{00}), and for most tuning conditions, to one axial mode. The reflectivities of the mirrors greater than 99.9 percent and 99.5 percent have been chosen to yield maximum power output of about 300 microwatts from one end of the laser. The laser resonator is machined from cast invar which was chosen for its low thermal coefficient (5×10^{-7} per degree centigrade). The geometry of this resonator is that of a "negative dumbbell" (a dumbbell being large at both ends and small at the center - - then a negative dumbbell is large at the center and small at both ends).

This shape concentrates the mass and stiffness near the center thereby reducing the transverse vibration of the mirrors. This geometry allows the fundamental longitudinal vibration mode of the resonator to have a node at the center. The entire resonator structure is supported at this node. This inhibits excitation of the longitudinal mode by disturbances in the support structure. The ends have been ground flat and parallel, permitting alignment of the cavity mirrors without angular adjustments. For alignment, a small translation of the mirrors is made by sliding the end plates; tightening the holding screws then locks the mirrors securely. The plasma tube is held in the resonator at each end by three screws which bear on invar collars attached to the tube. The entire resonator structure is housed in a thick wall cylindrical aluminum case which has antireflection coated windows at both ends. This case is hermetically sealed and provides isolation of the laser against pressure changes.

The plasma tube is 10 cms long and has a bore diameter of 1 mm. The tube is filled with He^{3}-Ne^{22}, and operates at $\lambda = 6328\text{Å}$. The plasma tube is entirely surrounded by a copper heat sink and has air shields around the Brewster windows. The heat sink is thermally and mechanically isolated from the invar resonator. This enables the heat generated in the tube (about 8 watts) to be conducted directly to the outer casing without adversely affecting the resonator.

The laser frequency is tuned by a piezoelectric transducer which moves one of the mirrors. The transducer consists of a stack of four ceramic (PZT-5) wafers, mechanically in series and electrically in parallel. These transducers have a tuning sensitivity of 3 MHz per volt.

2. Reference Cavity

The control systems use the passive resonator reference cavity as a Lipsett-Lee off axis discriminator. This discriminator, see Appendix A, has two advantages over using the cavity as an on axis discriminator. First, it is a circulating resonator rather than a Fabry-Perot type cavity, and thereby eliminates the problem of coupling between it and the laser cavity due to back reflection of light. Second, because frequency shifts in the laser result in changes in the output beam direction, it is not necessary to modulate the laser frequency over the resonance (as in the "Lamb Dip" servo) to generate an error signal. This is important for the many applications where an unmodulated output frequency is desired.

The reference cavity is a fused silica structure with a mirror separation of 10 cm. It is of the same general shape ("negative dumbbell") as the laser resonator. A hole has been drilled along the axis for the light, and another hole drilled to the outside to connect the interior optical path between the mirrors with an outside vacuum pump, which enables the cavity space between the mirrors to be evacuated to a pressure below 10 microns. The mirrors are connected to the ends of the fused silica cavity by epoxy, in a manner similar to that used for attaching Brewster angle windows to laser plasma tubes. The resonator is isolated within an aluminum housing similar to, but shorter than, that used around the laser, (see number 4 of figure 1). Both end faces of the housing have antireflection coated windows for letting light in and out of the resonator. The housing is hermetically sealed and an evacuation fitting is brought to the outer case.

3. Optical Train for Deriving Error Signals

A Lipsett-Lee off axis discriminator only passes radiation having a frequency near that of the resonance frequency, and then in a direction that is dependent on the frequency of the incident radiation. For example, suppose the incident radiation ω_R is equal to the resonant frequency and on emerging from the cavity it is incident on the screen at a point. If the incident radiation changes to $\omega_{R-} < \omega_R$ then on emerging from the cavity it is incident on the screen to the left of this point. Likewise for $\omega_{R+} < \omega_R$ it will be incident to the right of this point. This change in direction of the emergent beam due to change in frequency of incident beam is converted to frequency error signal by the optical train shown in figure 3.

Light leaving the resonator is divided vertically into two orthogonally plane polarized components by a split polarization rotating plate. These components then pass through a quarter-wave retardation plate and are transformed to left and right circularly polarized components. The phase modulator produces two orthogonally plane polarized components which are switching at the modulation frequency. The intensity of each component depends on the intensity of the light transmitted by each half of the split plate and the phase of the modulation cycle. The light then passes through a linear polarizer oriented at 45 degrees to the plane polarized components.

If equal amounts of light are passing through the halves of the split plate (correspondent to incident frequency equal to resonant frequency), there will be no resulting intensity modulation during the course of the modulation cycle. If more light is passing through one half of the

split plate than the other (correspondent to incident frequency different from resonant frequency, since the beam emerging from the cavity is centered on the split plate), there will be an intensity modulation. The phase of the intensity modulation, with respect to the modulator drive signal, is determined by which half of the split plate is transmitting more light. The light now is incident on an RCA 8645 photomultiplier. All the information needed to derive the frequency error signal is contained in the photomultiplier output current.

The modulator consists of a 2.5 x 2 x 1 cm solid block of fused silica to which is cemented a piezoelectric wafer driven at the mechanical resonance frequency. Driving the block at its mechanical resonance permits excitation of a vibrational mode using only a small amount of power. The vibration of this block results in an alternate compression and expansion along axes perpendicular to the light path. This causes a strain induced birefringence which varies at the 100 kHz modulation frequency.

4. Electronics Module

There is a separate electronics module for both laser systems. The electronics module, shown in figure 4, contains the laser power supplies, temperature controller electronics, the servo system for slaving the laser to the passive cavity, and various power supplies for the entire system. The top panel contains plasma tube power supplies which are controlled by the adjustments on the second panel from the top. The third panel from the top contains the photomultiplier power supply and is adjusted by its built in controls. The fourth panel from the top contains the proportional temperature controllers. This is a two stage

controller which regulates the temperature of the laser housing and the reference cavity. The first stage of this two stage (tandem) controller adds about 50 watts of power to the large external system housing to raise its temperature about 15°C above the ambient room temperature. The second stage adds an additional 10 watts directly to the reference cavity enclosure to raise its temperature about 10°C above the surrounding housing temperature, i.e., about 25°C above ambient. The amount of heat added to each stage varies in inverse proportion to the temperature measured by separate sensors. The residual temperature drift is about ±0.005°C per hour. This is caused in part by instabilities of the thermistor sensors, and in part by residual thermal gradients. Directly beneath the temperature controllers is the servo electronics panel. The servo electronics package consists of the following circuitry:

a. 100 kHz modulator drive oscillator.

b. Synchronous detector with a carrier frequency of 100 kHz, and a band width of approximately 1 Hz.

c. Driver amplifier which is used to actuate the piezoelectric mirror transducer in the laser.

d. Switching circuits to select each of the three modes of operation previously described.

The servo electronics has been designed for low noise and hum, and small direct current drift. The range of the servo system is ±300 MHz which is adequate to slave the laser to the reference cavity for a period of several days without resetting the laser frequency. The lowest two panels on the module are then 15 volt and 300 volt supplies, common to the entire system.

IV. DESCRIPTION OF EXPERIMENTAL ARRANGEMENT

Figure 5, with its overlay, is a photographic display of the experimental arrangement used and allows for a listing of the experimental equipment as follows:

1. Laser unit number 1
2. Laser unit number 2
3. Electronic console for unit number 1
4. Electronic console for unit number 2
5. Isolation table
6. Trap for vacuum system
7. Beam splitter
8. Phototube
9. Wideband amplifier and external filter
10. Converter plug-in unit for Hewlett-Packard Counter
11. Hewlett-Packard Counter
12. Hewlett-Packard Digital Recorder
13. Wideband amplifier
14. Power supply for wideband amplifier
15. Local oscillator
16. Oscilloscope and mixer
17. Analog chart recorder

The equipment displayed by figure 5 was not all used at one time, but was the total equipment used for two different measuring techniques to be described later.

Figure 6 shows the orthogonality and alignment of the beams from laser units numbers one and two, and their incidence on the phototube.

Laser unit number one is located in the center of the photograph; unit number two is to the left and out of the figure. Beam number one is clearly visible in its incidence on and transmission through the beam splitter. Half of this intensity seen transmitted through the beam splitter comes from unit number two. If one looks closely at the left face of the beam splitter one can see the incident radiation from unit number two. Since these beams are all in the same plane, half of each beam is made incident on the face of the photomultiplier tube. This incidence may be seen if one observes the face of the phototube quite closely. This photograph of the beams was made possible by blowing smoke in the path of the beams. Due to the non uniformity of the smoke, one of the beams did not show up clearly. When the blanket of smoke was more uniform the beams appeared to be of equal intensity, which in fact they were.

Two slightly different measuring techniques were used to obtain data on the laser stability. The essential difference between the two techniques is the method used for heterodyning the received signal prior to the recording of data. A block diagram of the technique using an external local oscillator and mixer in the heterodyning section is given in figure 7. Figure 8 gives a block diagram of the second technique which uses a frequency converter plug-in unit in conjunction with a stable counter as its heterodyning section. The first technique using the external oscillator proved to be less accurate than the second technique, due primarily to the drift in the external local oscillator. An analysis of the accuracy of test equipment will be given later. Due to the similarity of the two techniques and since technique number two was more accurate and therefore the most used technique, only this method

will be described in detail.

In an effort to reduce all external vibrations, as much as possible, the laser units were placed on an isolation table. The table was supported by four columns, each comprised of an outer sleeve with an internal cylinder. The cylinder was attached to the table and compressed air between the sleeve and the cylinder supported the table on a virtual "column of air." This served to isolate the table from vibrations greater than 1 Hz. Further, this table had the capability to keep its alignment to within one second of arc. The vacuum pump, shown in figure 8, was used to reduce the pressure in the external reference resonant cavities to less than ten microns. The trap, between pump and cavities, was necessary to protect the optical surfaces of the cavity from oil and particles present in the pump.

Radiation from lasers one and two were aligned in the same plane and made incident on the phototube. The conditions for optical mixing at the phototube were maximized using an oscilloscope. The output or "beat" signal from the phototube was amplified and filtered where it was coupled to the input of the frequency converter. The counter then counted the converted frequency and provided a digital input to the recorder which printed out a permanent tape of the data.

The frequency converter mentioned above is a heterodyne frequency converter containing four basic functional sections: harmonic generator, harmonic selector cavity, mixer, and video amplifier. In normal operation the harmonic generator produces all of the harmonics of 10 MHz between 50 and 500 MHz. The harmonic selector cavity is tuned to select one of these harmonics to be supplied to the mixer. The mixer output is the

difference frequency produced by the mixing of the input frequency and the frequency supplied by the harmonic selector cavity. This difference frequency is amplified by the video amplifier and supplied to the counter input circuit.

V. EXPERIMENTAL INVESTIGATION

A. Description of Tests Performed

The essential difference between the two arrangements described in the last section was in the electronic heterodyne section of the data system. Using these two experimental arrangements, two tests on relative frequency stability were performed; the long term and short term frequency stability. With these arrangements as previously described, the data collected on long term and short term stability was for the condition of closed loop, i.e., with the servo operative. A number of tests or runs of this type were recorded. The long term stability test was the result of a frequency sampling every minute for a period of six hours, producing a total of 360 data points. Utlizing this data, a computer program was written which provided the following results for the long term tests:

a. The average frequency

b. The standard deviation about this average frequency, σ_{ave}

c. The maximum frequency and minimum frequency occurring during the entire run

d. The initial frequency

e. A least mean square fit of the form $y = a + b\,x$

f. The standard deviation about this line, σ_{LMS}

g. The slope of this line

h. Two different methods for hourly drift rates

The short term stability test was the result of a frequency sampling every ten seconds for a period of one hour, again producing a total of

360 data points. From this data the computer program provided the same parameters as for the long term tests with the exclusion of hourly drift rates.

In an effort to show the effectiveness of the servo system, a long term test and a short term test were taken in the open loop mode. This is the arrangement as before with the servo system switched out of the circuit. The stability now is just a function of the Fabry-Perot Laser Cavity itself. The long term test here was 2 1/2 hours only, not six as for closed loop. The computer program provided the same parameters for open loop long term and short term test as before for closed loop long and short term tests.

B. Accuracy of Test Equipment

A confidence in the data obtained through the use of the converter and local oscillator test arrangements (see chapter IV), could be secured only through a knowledge of the inherent drift of these two pieces of equipment. A Hewlett-Packard Frequency Synthesizer was used as a constant frequency reference. This constant frequency was used as an input to the mixer and the local oscillator was the other input. The output of the mixer was monitored for a period of one hour providing short term stability test data, and for a period of four hours providing long term stability test data. This data on the local oscillator stability was analyzed as before and the results are shown in table I (all frequency units are kHz).

Using the constant frequency reference as the input to the converter then monitoring the output provided a test of the stability of the converter arrangement. This proved to be most accurate. It

produced a constant output frequency ± one Hz (table I).

The hourly drift rates for the local oscillator obviously are not negligible, the highest drift rate observed for the local oscillator being approximately 33% of the average laser drift rate for closed loop mode. The maximum spread of frequency,

$$\Delta \nu = \nu \text{ max} - \nu \text{ min}$$

is 133 kHz.

The results of table I clearly indicate that the converter test arrangement is the more accurate test arrangement. While this is true, two runs of long term and short term results using the local oscillator test arrangement are given in the final results, primarily for comparison.

VI. DISCUSSION OF RESULTS

A. Long Term Stability

Analysis of data for the long term stability tests produced the results tabulated in table II. There are nine different quantities found for each of the six long term runs. These quantities will be discussed in succession.

Average Frequency, $\bar{\nu}$

The average frequency is expressed mathematically as:

$$\bar{\nu} = \frac{1}{n} \sum_{i=1}^{n} \nu_i \qquad (1)$$

$$n = 360$$

Standard Deviation, σ_{ave}

The deviations or residuals, (δy_i), of the points of each set about its average frequency were used to produce the standard deviation given by

$$\sigma_{ave} = \left[\frac{\sum_{i=1}^{n} (\delta y_i)^2}{n-1} \right]^{1/2} \quad \text{where} \quad \delta y_i = (y_i - \bar{y}) \qquad (2)$$

$$n = 360$$

The standard deviation is considered the worst probable deviation from the average, i.e., approximately 68% of the deviations will be less than this specified value. From the tabulated values we see that the largest value of σ_{ave} = 487.156 kHz was for run number 5. This was for the open loop case, and expected to be the worst case. The smallest value of σ_{ave} = 70.510 kHz was for run number 1, but this must be discounted due

to drift in the local oscillator explained earlier. The lowest value of σ_{ave} = 114.848 kHz for run number 3 using the converter arrangement is approximately four times smaller than that for the open loop case. Even the largest value of σ_{ave} = 205.379 for the converter arrangement is smaller than the open loop case by a factor of approximately two. (The difference between servo controlled and open loop case will be even more dramatic when the standard deviation of least squares fit is considered.)

Maximum and Minimum Frequency

This is the single highest and single lowest values of frequency recorded during a given test. The difference between these two values is the peak to peak excursions or the maximum spread, i.e.,

$$\Delta \nu = \nu_{max} - \nu_{min} \tag{3}$$

For a given run this maximum spread describes the maximum peak to peak envelope of the individual deviations. This maximum spread provides the linear ordinate for the frequency versus time plots of the long term runs, figures 9 through 14. As seen in the figures this maximum spread ranges from 314 kHz to 2038 kHz. Here again for the open loop case, the maximum spread is greater than that for the converter case by a factor of approximately 3.5.

A presentation of the long term stability data in histogram form is given for the six runs by figures 15 through 20.

Initial Frequency, ν_1

This is simply the first frequency reading obtained at the start of each test.

Slope, φ

Using the method of least mean squares, a curve of the form

$$y = a + b\,x \tag{4}$$

was fitted to the data. The coefficient a is the value of the y intercept and b is the slope of the line fitted to the data. This slope has the units of kHz/hr. Values of this slope for all six runs are tabulated in table II. Considered alone this value may be misleading. To get a true picture one must consider the maximum spread and standard deviation of least fit along with the slope. The non smoothness of the data of figures 9 through 14 bear this out.

Standard Deviation, σ_{LMS}

This is again just the result of the deviations about the least mean square fit. It is considered the worst possible deviation from the least square fit, i.e., approximately 68% of the deviation will be less than the specified value.

Note that run number 5, the open loop case, has a slope φ = 8.00 kHz/hr but a σ_{LMS} = 487.197 kHz. Therefore, since the slope is so small, it might be misleading without a knowledge of its extreme value for deviations. As before, the local oscillator case has the smallest value of σ_{LMS}, but as before, it falls suspect due to its inherent drift. In any case, the difference between the σ_{LMS} for the converter and local

oscillator case is slight. However, the σ_{LMS} for the open loop case is greater than that for the converter case by a factor of from 4 to 6.

Hourly Drift Rates, D_I, D_{II}

We come now to what is probably the most important single result, the hourly drift rate. The hourly drift rates D_I and D_{II} were found using two different averaging methods. Hourly drift rate D_I was the result of taking the average of five readings occurring at the end of each hour; then taking the difference between each two successive five minute averages. Hourly drift rate D_{II} was the result of taking an average over all the points for each hour to obtain a value that corresponds to the middle of the hour; then taking the difference between each two successive one hour averages.

The largest value of D_I = 4.645 MHz/hr occurs for the open loop case; correspondingly the largest value of drift for the converter cases is D_I = 285.9 kHz/hr. This corresponds to a ratio greater than 16, i.e., the use of the external reference cavity improves the drift performance of the system by greater than an order of magnitude. Taking the best value, i.e., the smallest value, of D_I for the open loop case and the smallest value for converter case, one finds a ratio of approximately 50, and again the performance improvement is greater than an order of magnitude through the use of the external reference cavity.

Comparison of the open loop case with the converter case for the hourly drift rate D_{II}, one finds the largest open loop value of D_{II} = 5.150 MHz/hr and the largest converter value of D_{II} = 433 kHz/hr; a factor of approximately 12, or again greater than an order of magnitude. The value of D_{II} = 433 kHz/hr is felt to be due to a drastic ambient

temperature change occurring in the laboratory between the third and fourth hour of this test. Noting figure 13, this is indicated by the unduly steep negative slope in the data at this period. From comparison to the other hourly drifts of D_I and D_{II}, it is felt that this figure of 433 kHz/hr probably should be adjusted to approximately 300 kHz/hr.

If, as before, we take a comparison of the lowest value of D_{II} for open loop and for converter case, we find a ratio of approximately 150, i.e., greater than two orders of magnitude drift improvement due to use of the external reference cavity.

It appears that the hourly drift rate D_{II} might present a more meaningful representation since it uses a larger number of data samplings in its averaging process and thereby gives a more probable value of drift rate. In either case, the largest value of drift rate found for the converter case does not exceed 300 kHz/hr (allowing the corrected value from run 11).

The long term stability measured by this experiment has been relative stability between two lasers and any frequency drift suffered by the two lasers simultaneously has gone undetected. For this experiment $\lambda = 6328\text{Å}$, therefore

$$\nu \approx 4.74 \times 10^{14} \text{ Hz} \tag{5}$$

using this frequency and noting the value of the variations, the best long term relative stability is of the order of a few parts in 10^{10}.

B. Short Term Stability

Data on short term stability was analyzed to produce the results tabulated in table III. These quantities will be discussed in succession

Average Frequency, $\bar{\nu}$

The average frequency is expressed mathematically as:

$$\bar{\nu} = \frac{1}{n} \sum_{i=1}^{n} \nu_i \qquad (6)$$

$$n = 360$$

Standard Deviation, σ_{ave}

Using the deviations about the average frequency, we have

$$\sigma_{ave} = \left[\frac{\sum_{i=1}^{n} (\delta y_i)^2}{n-1} \right]^{1/2} \qquad (7)$$

where $\delta y_i = (y_i - \bar{y})$

$$n = 360$$

Most of the deviations, i.e., 68% will fall within the value specified by this standard deviation. Run number 6 for the open loop case produced the largest value of σ_{ave} = 252.037 kHz. The smallest value of σ_{ave} = 31.181 kHz was for run number 2. This, however, was the local oscillator case and falls suspect due to the inherent drift in the local oscillator. The smallest value of σ_{ave} = 31.574 kHz for a converter arrangement is approximately equal to that for the local oscillator and occurs for run number 10. This value is approximately 8 times less than that for the open loop case. Even the largest standard deviation for a converter arrangement (σ_{ave} = 70.573 kHz, run number 4) is still smaller by a factor of 3 than that for the open loop case.

Maximum and Minimum Frequency

This is the simple highest and lowest value of frequency recorded during the test and whose difference

$$\Delta \nu = \nu_{max} - \nu_{min} \tag{8}$$

produces the peak to peak excursions or maximum spread. This maximum spread describes the peak to peak envelope of the individual deviations and provides the linear ordinate for the frequency versus time plots of the short term stability runs, figures 21 through 26. As evidenced by these figures the maximum spread ranges from 147 kHz to 830 kHz. If the maximum spread for the open loop case is ratioed to that for the converter arrangements, the open loop case is seen to be greater by at least a factor of 5.

A presentation of short term stability data is found in histogram form in figures 27 through 32.

Initial Frequency, ν_1

This is simply the first frequency reading obtained at the start of each run.

Slope, φ

Using the method of least squares a curve of the form

$$y = a + b\,x \tag{9}$$

was fitted to the data. The coefficient b is the slope of this fitted line; coefficient a is its y intercept. The slope has the units of kHz/hr. Values of this parameter for all six runs are tabulated in table III. The slope, to be meaningful, must be considered in conjunction with such parameters as maximum spread and the standard deviation of best fit, i.e., σ_{LMS}.

Standard Deviation, σ_{LMS}

Most of the deviations about the least square fit, i.e., 68% will be less than the tabulated value of σ_{LMS}. For the six short term runs this parameter ranges from 14.9 kHz to 108.2 kHz. The σ_{LMS} for the open loop case is greater than 2 times that for the converter arrangements.

Again we have only measured relative stability between two lasers. Using

$$\nu \approx 4.74 \times 10^{14} \text{ Hz} \tag{10}$$

and the deviations discussed the short term relative stability is of the order of a few parts in 10^{11} at best.

VII. CONCLUSIONS

Relative frequency stability between two lasers has been measured, therefore, any frequency drift suffered by the two lasers simultaneously has gone undetected.

The use of the external reference cavity as a passive frequency reference improved the drift over that found for open loop case by a figure greater than one order of magnitude and in one case as great as 2 1/2 orders of magnitude.

The system was found to have the following specifications:

Laser output power	$\gtrsim$ 100 microwatts
Plane of polarization	Electric Vector Vertical
Laser wavelength	6328Å

Open loop drift rate, D_o

$$600 \ \frac{kHz}{hr} \lesssim D_o \lesssim 5 \ \frac{MHz}{hr}$$

Closed loop drift rate, D_c

$$6 \ \frac{kHz}{hr} \lesssim D_c \lesssim 300 \ \frac{kHz}{hr}$$

Linewidth 20 kHz

The long term relative stability was found to be of the order of a few parts in 10^{10}.

The best short term relative stability was one order of magnitude better, i.e., a few parts in 10^{11}.

TABLE I

RESULTS OF STABILITY ANALYSIS OF TEST EQUIPMENT

	$\bar{\nu}$	σ ave	νmax	νmin	ν_1	Φ	σ LMS	D_I	D_{II}
LONG TERM LOCAL OSCILLATOR TEST	6282.63	27.465	6396.41	6263.19	6320.39	-26.85	26.159	-44.791 -10.051 -2.823	-98.140 -17.071 -4.204
SHORT TERM LOCAL OSCILLATOR TEST	6321.99	28.385	6396.41	6288.27	6368.71	-96.20	8.602		
CONVERTER TEST	FREQUENCY REMAINED CONSTANT ± 1Hz FOR 6 HOUR TEST.								

TABLE II

RESULTS OF LONG TERM STABILITY TESTS

RUN #	$\bar{\nu}$	σave	νmax	νmin	ν_1	Φ	σ LMS	D_I	D_{II}	COMMENTS
1	4528.11	70.510	4652.90	4338.80	4483.34	14.85	65.573	-124.883	-122.063	LOCAL
								111.176	-17.738	OSCILLATOR
								95.424	182.222	
								-42.540	-39.218	
								-117.348	-36.742	
3	9525.69	114.848	9790.42	9263.05	9603.00	-25.64	105.767	68.665	98.742	CONVERTER
								20.941	16.833	
								26.484	149.679	
								-177.080	-14.575	
								-198.955	-298.042	
5	5491.70	487.156	6439.00	4401.24	5487.64	8.00	487.197	595.648	919.419	CONVERTER
								-1250.180	-677.921	OPEN LOOP
								-4644.550	-5150.380	
9	4744.56	98.377	4952.44	4562.19	4839.90	331.62	81.431	-54.621	-48.443	LOCAL
								-170.414	33.798	OSCILLATOR
								6.266	-204.034	
								31.832	78.544	
								-38.520	-14.542	
11	6827.19	176.862	7195.71	6595.72	7069.83	-89.69	108.556	127.804	-5.833	CONVERTER
								-285.926	94.553	
								-124.310	-433.149	
								12.729	46.135	
								-267.897	-93.250	
13	608.20	205.379	1008.60	306.11	933.55	-107.89	81.854	-173.709	-57.198	CONVERTER
								-188.890	-163.417	
								-127.209	149.143	
								-61.341	-106.492	
								41.320	17.738	

TABLE III

RESULTS OF SHORT TERM STABILITY TESTS

RUN #	$\bar{\nu}$	σ ave	νmax	νmin	ν_1	Φ	σ LMS	COMMENTS
2	4524.87	31.181	4594.50	4447.50	4572.16	-94.84	14.922	LOCAL OSCILLATOR
4	9510.21	70.573	9636.24	9331.50	9422.51	175.89	49.016	CONVERTER
6	5347.08	252.037	5731.41	4900.85	4953.86	788.63	108.146	CONVERTER(OPEN LOOP)
10	4885.33	31.574	4968.47	4817.31	4855.14	60.55	26.295	LOCAL OSCILLATOR
12	6966.44	39.379	7046.69	6885.03	6993.79	-54.85	36.085	CONVERTER
14	957.59	39.400	1012.01	857.70	985.64	-56.26	35.898	CONVERTER

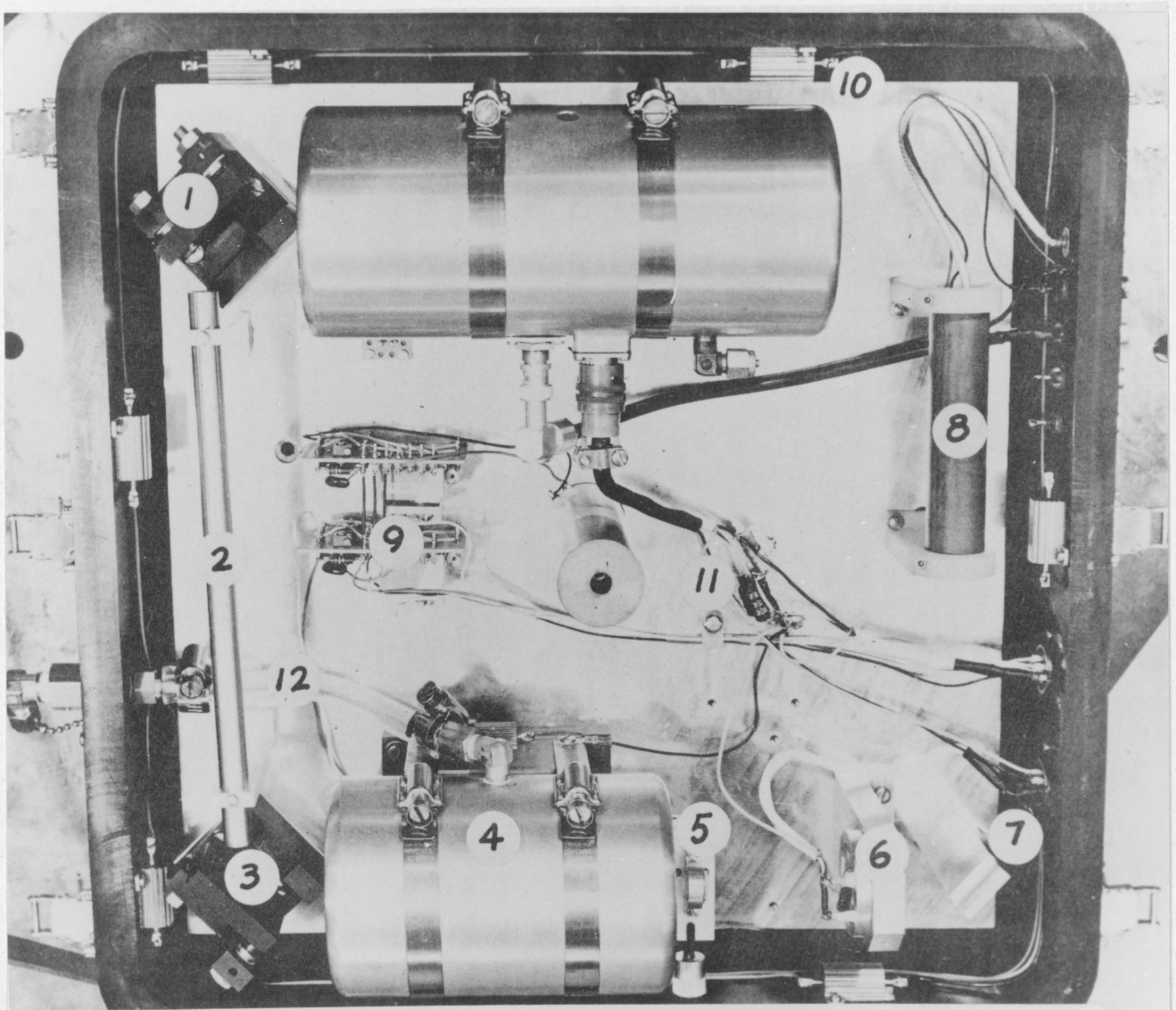

FIGURE I. LASER COMPONENTS

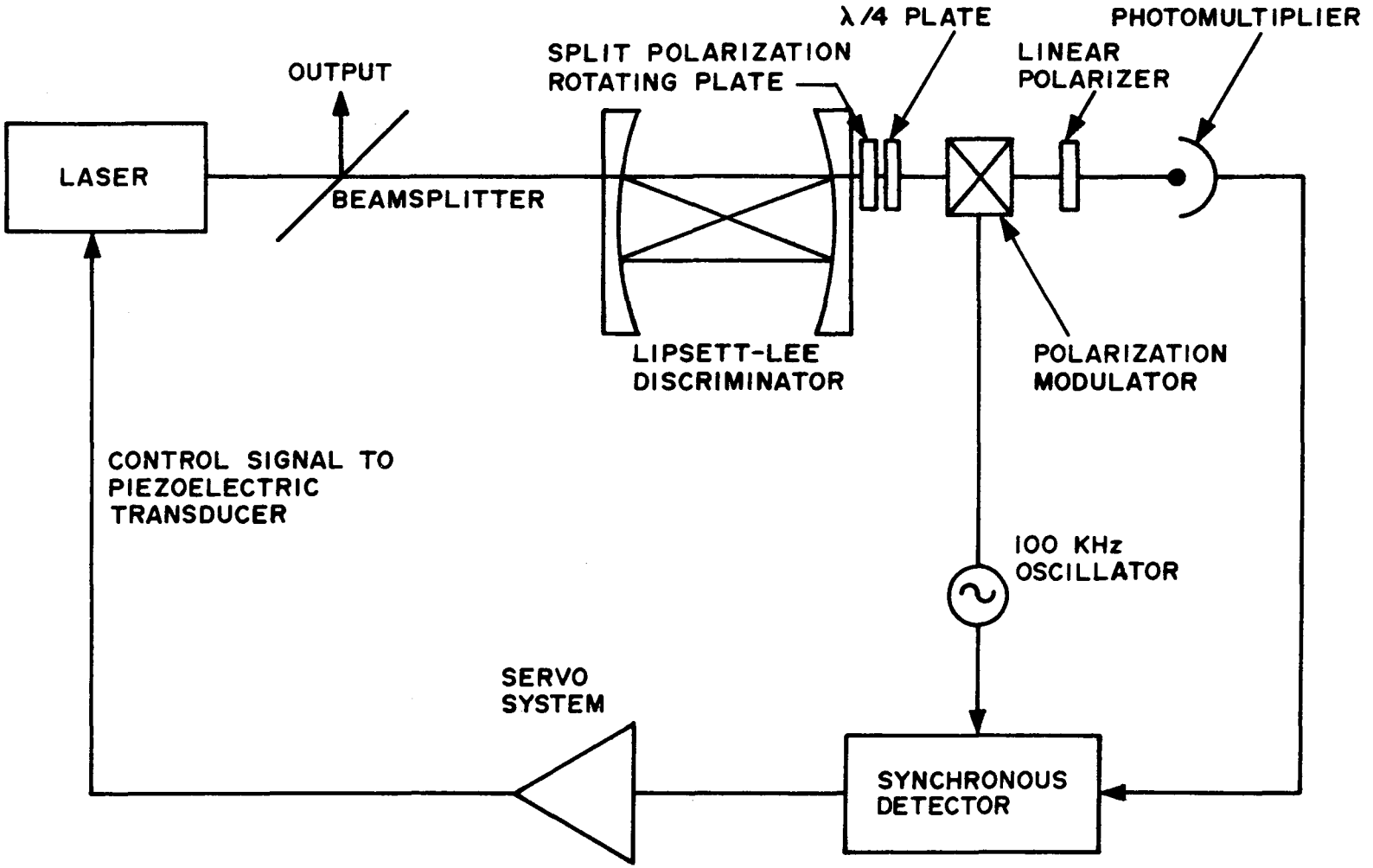

FIGURE 2 CLOSED LOOP FREQUENCY CONTROL SYSTEM

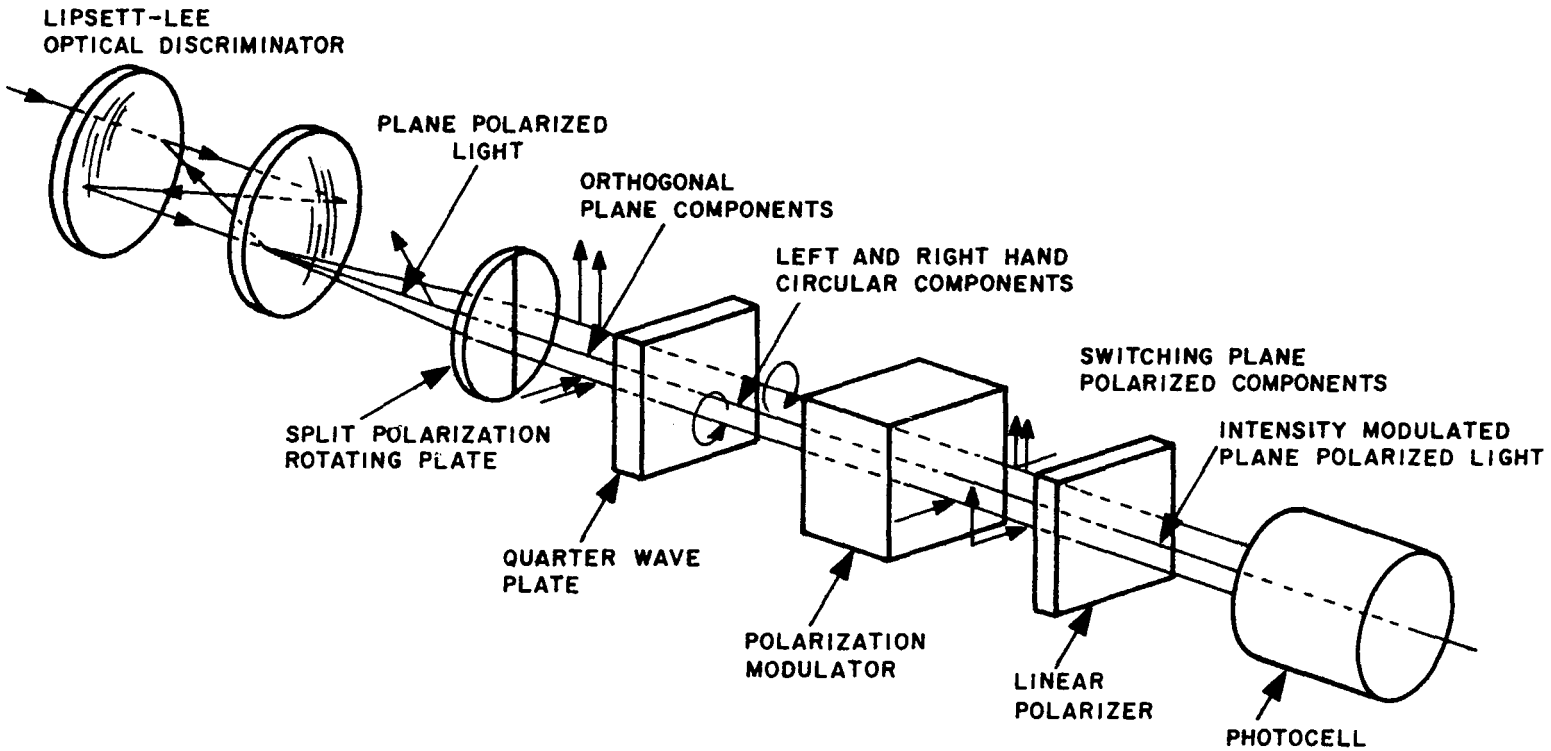

FIGURE 3 OPTICAL TRAIN FOR GENERATION OF ERROR SIGNAL

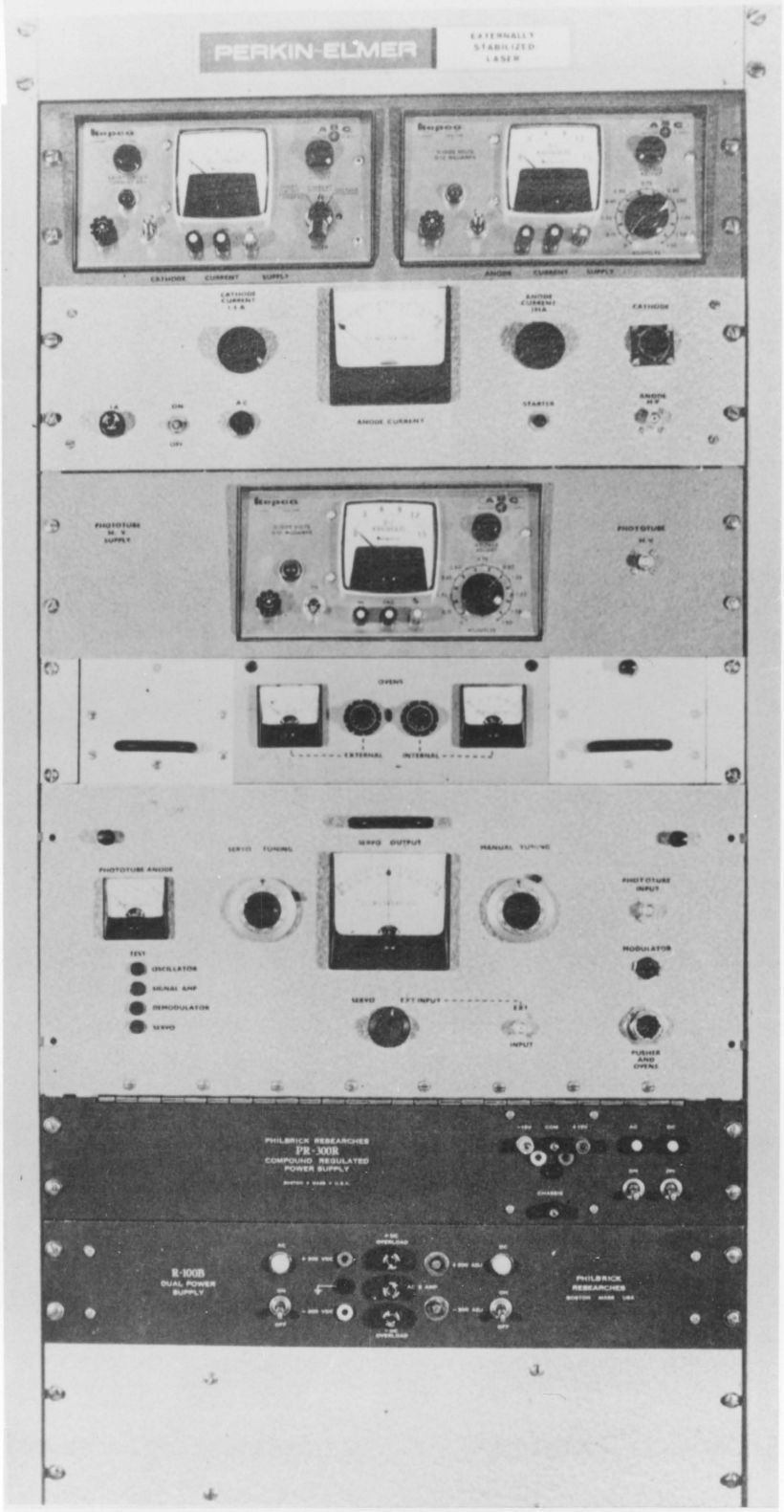

FIGURE 4. ELECTRONICS MODULE

FIGURE 5. EXPERIMENTAL ARRANGEMENT WITH OVERLAY

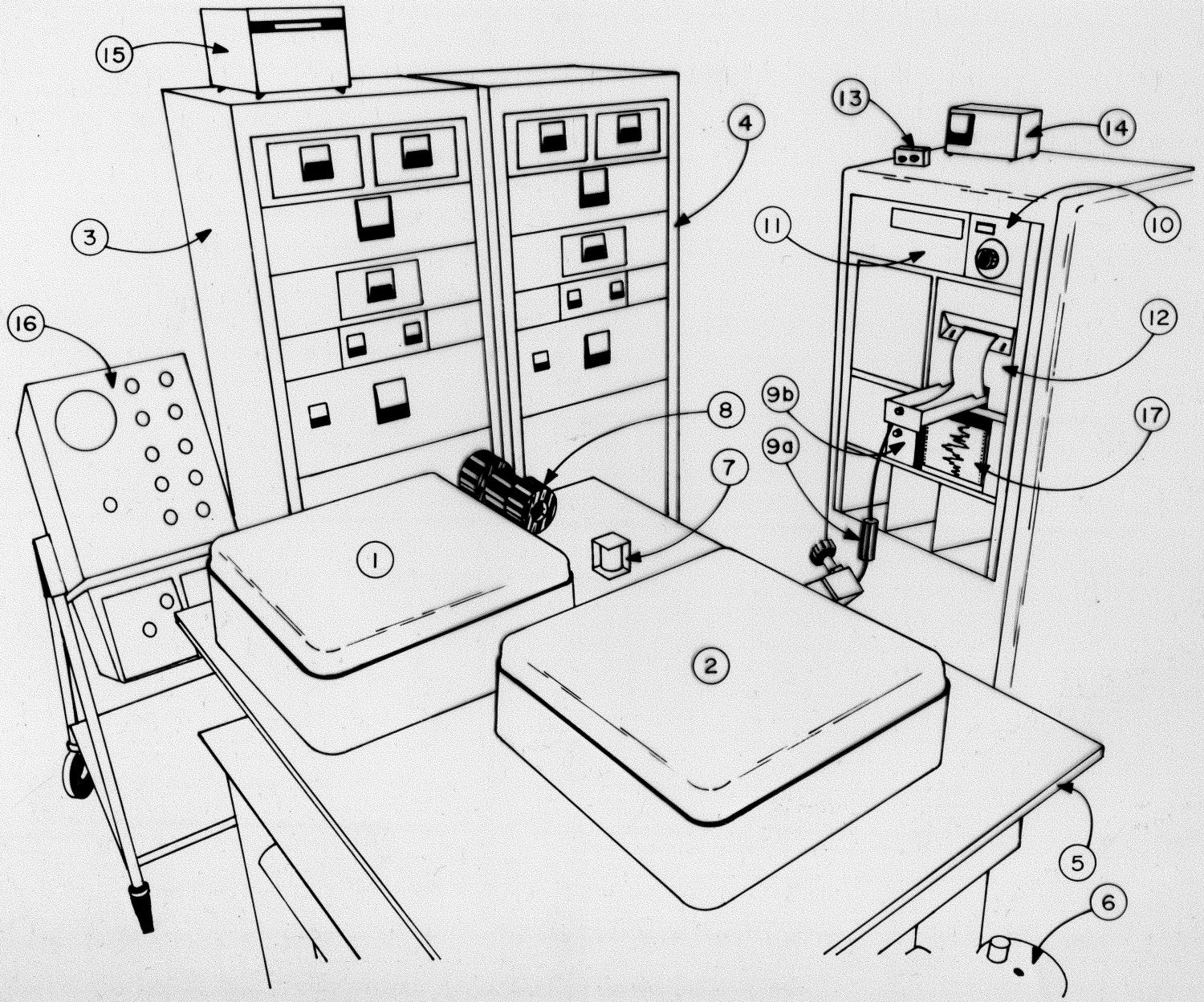
15
4
3
16
8
7
1
2
13
14
10
11
12
9b
17
9a
5
6

FIGURE 6. LASER ALIGNMENT PLANE

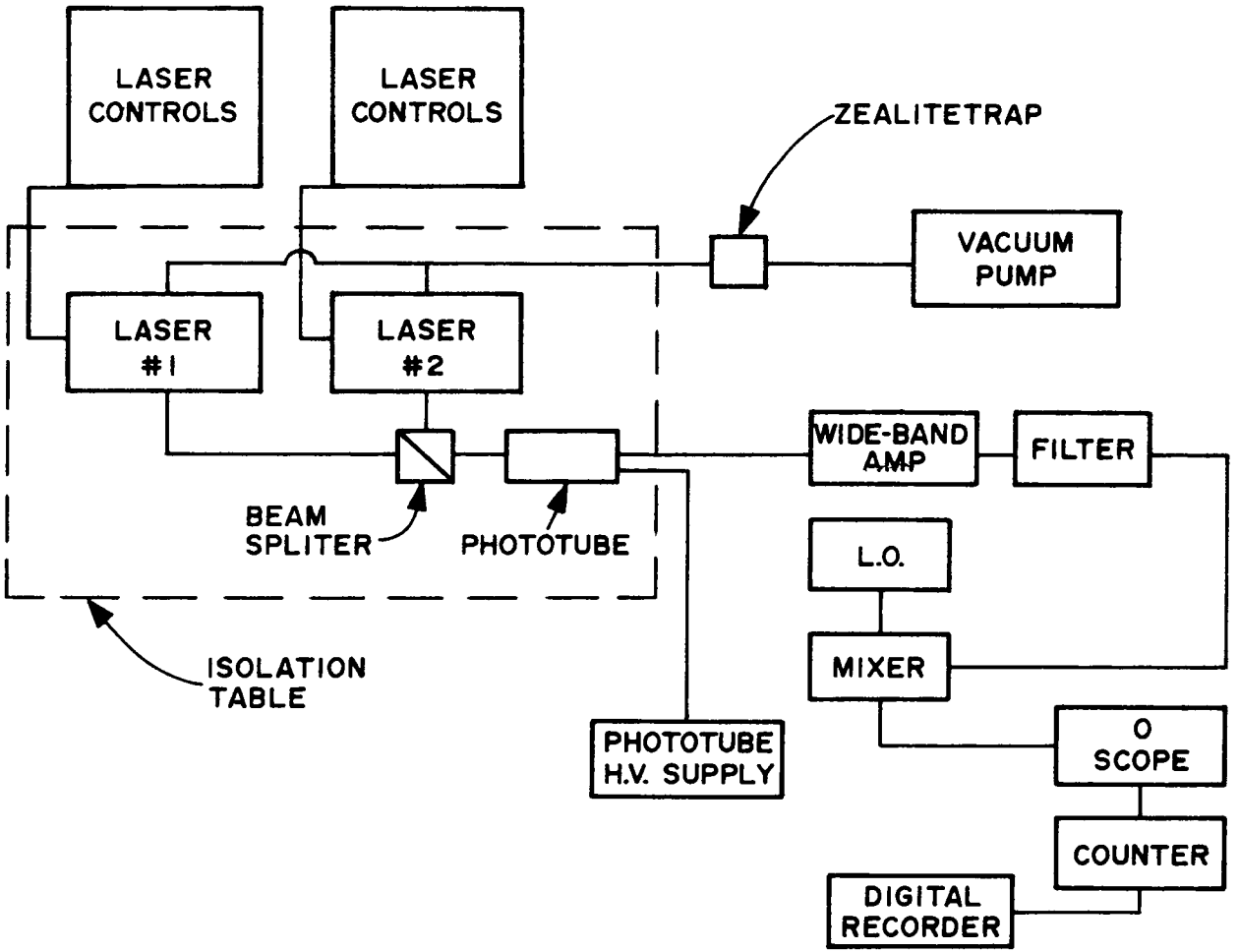

FIGURE 7 BLOCK DIAGRAM OF LOCAL OSCILLATOR ARRANGEMENT

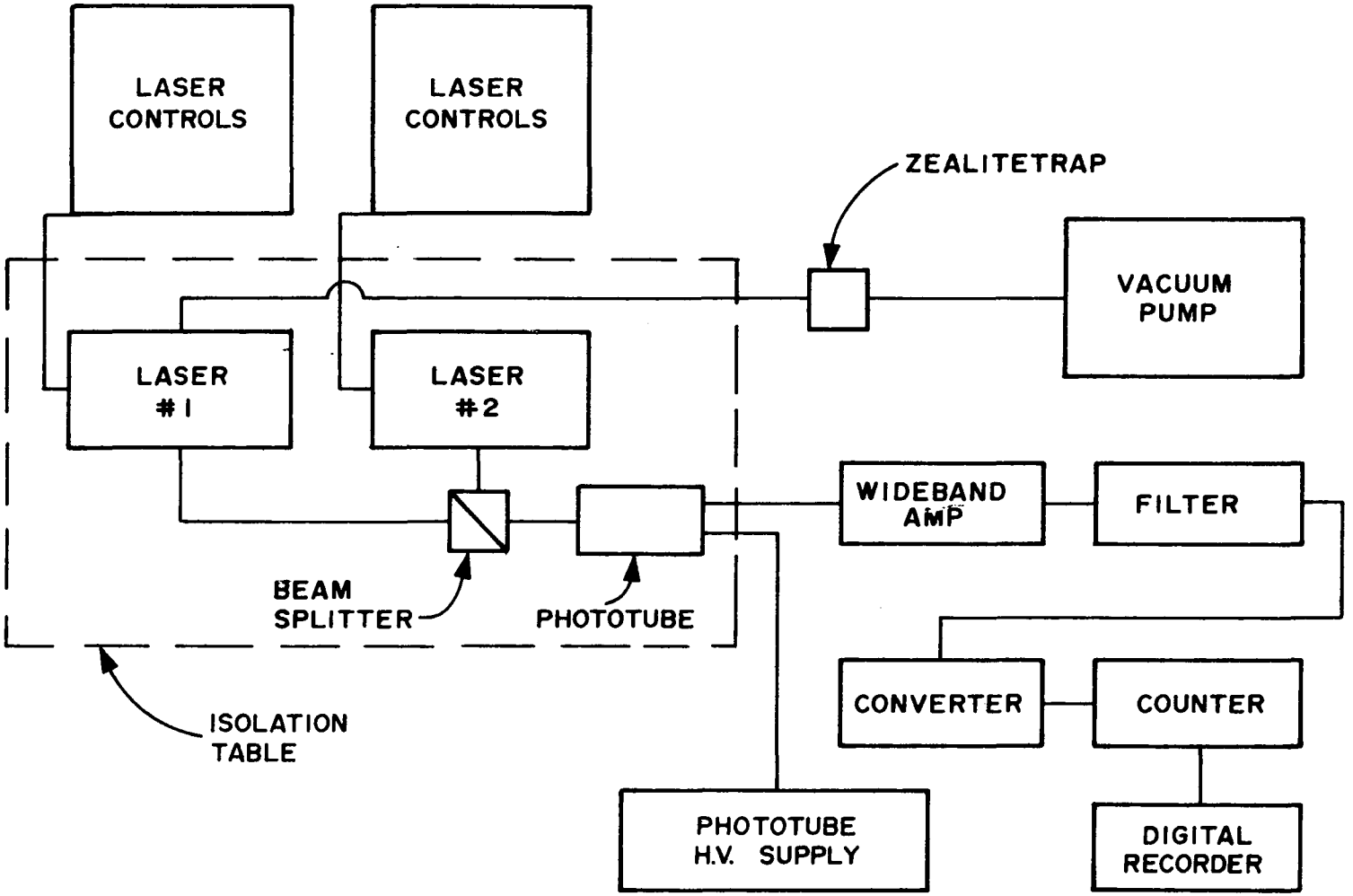

FIGURE 8 BLOCK DIAGRAM OF CONVERTER ARRANGEMENT

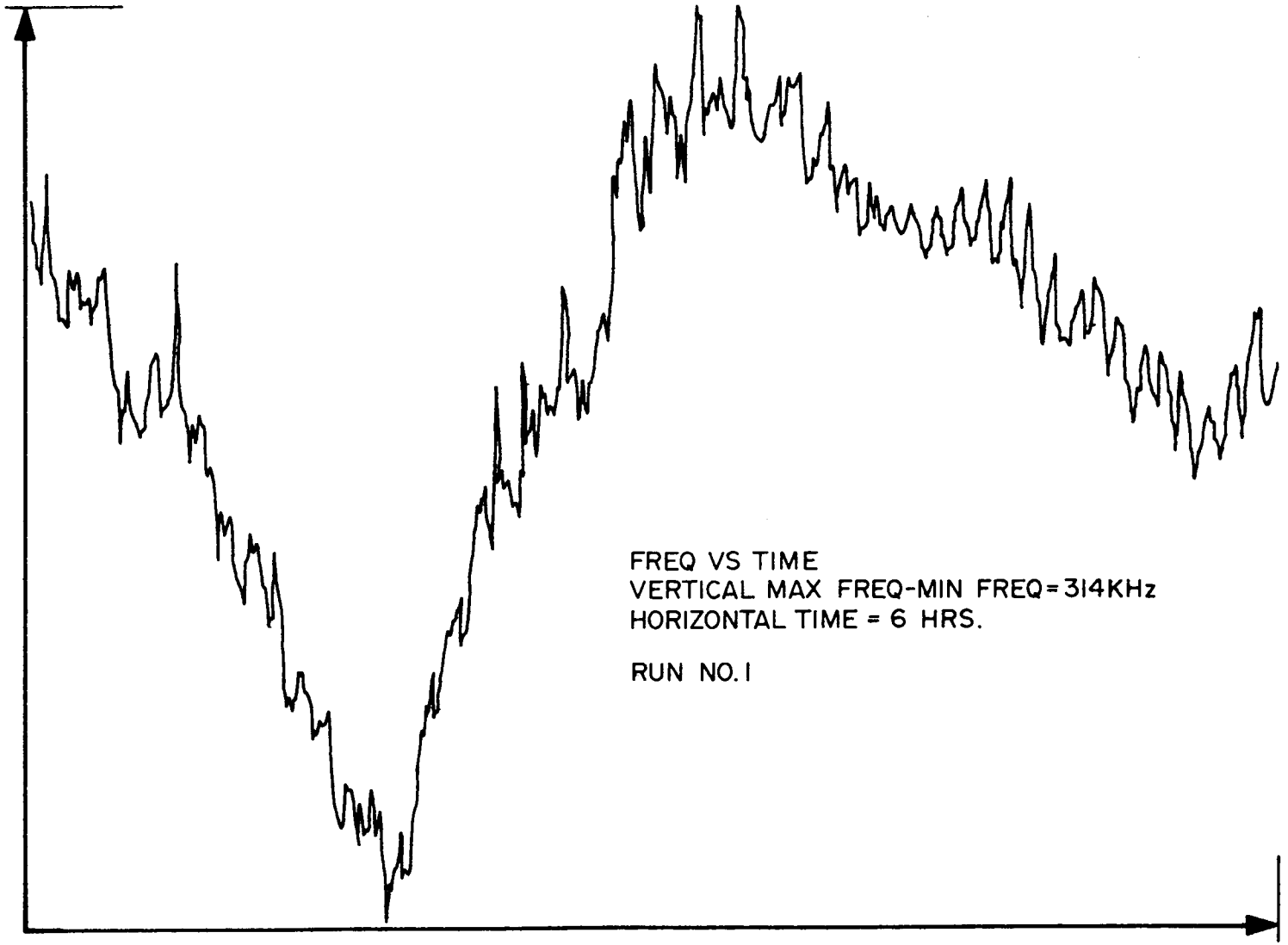

FIGURE 9 FREQUENCY VERSUS TIME (RAW DATA)

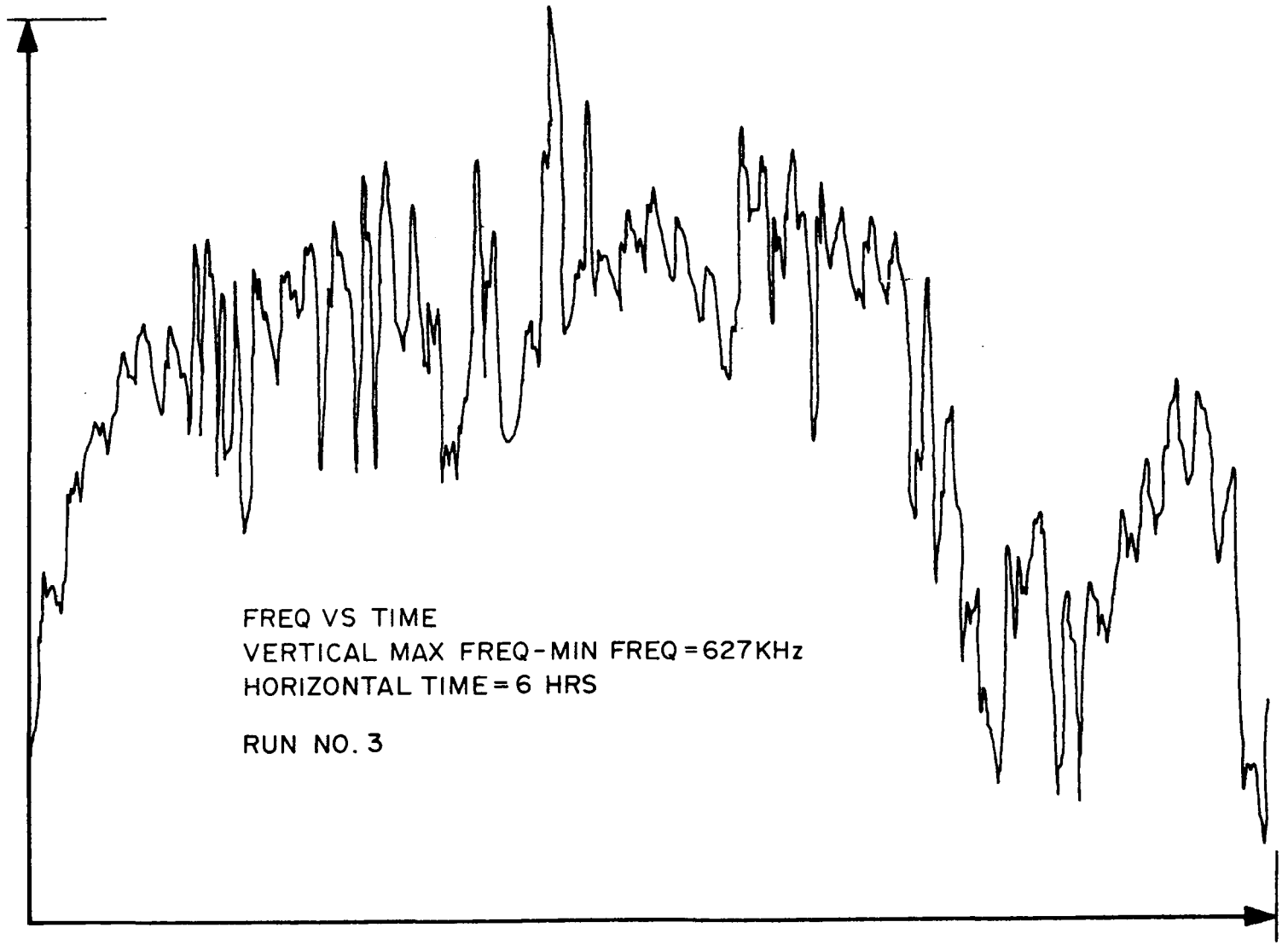

FIGURE 10 FREQUENCY VERSUS TIME (RAW DATA)

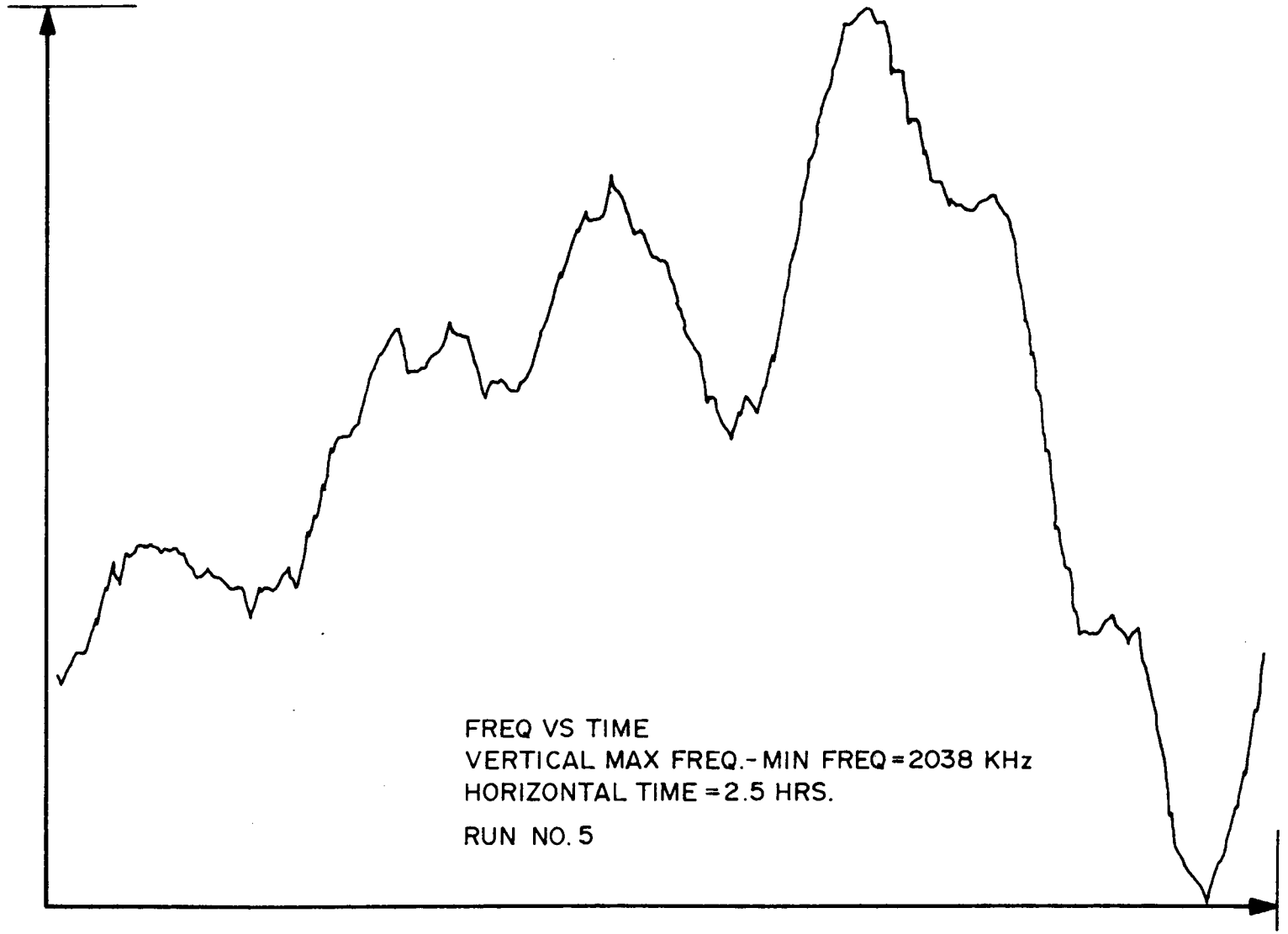

FIGURE 11 FREQUENCY VERSUS TIME (RAW DATA)

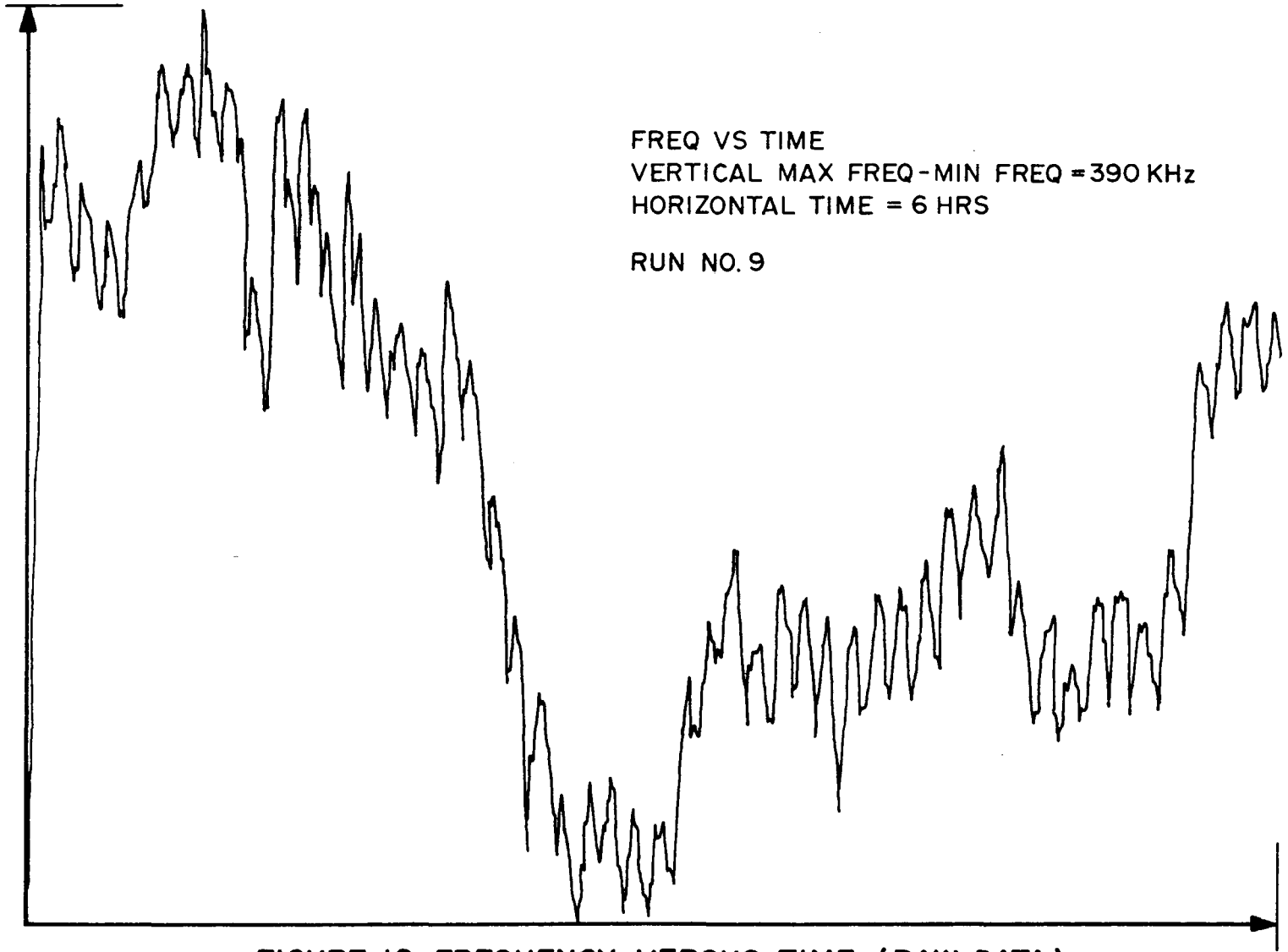

FIGURE 12 FREQUENCY VERSUS TIME (RAW DATA)

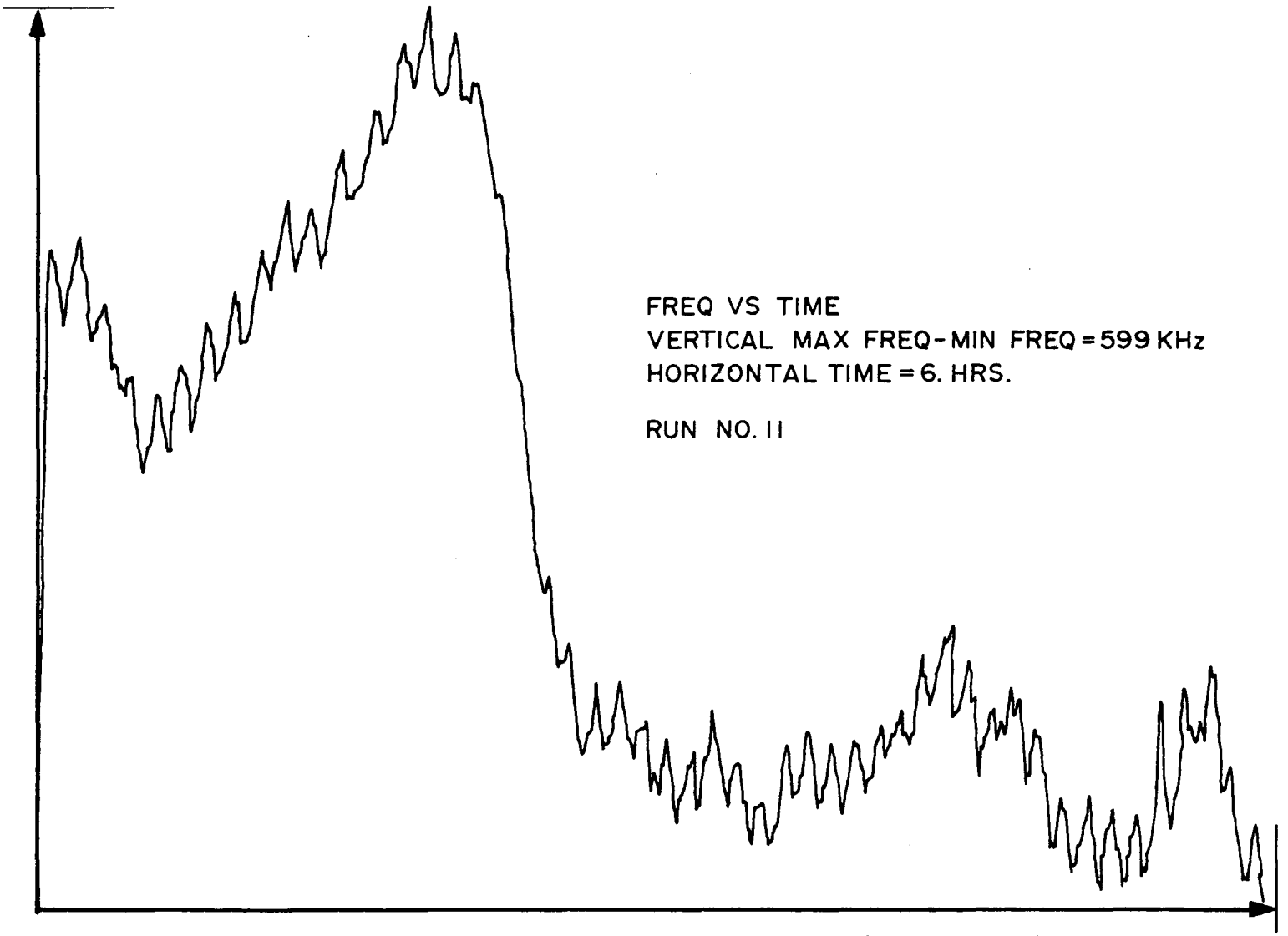

FIGURE 13 FREQUENCY VERSUS TIME (RAW DATA)

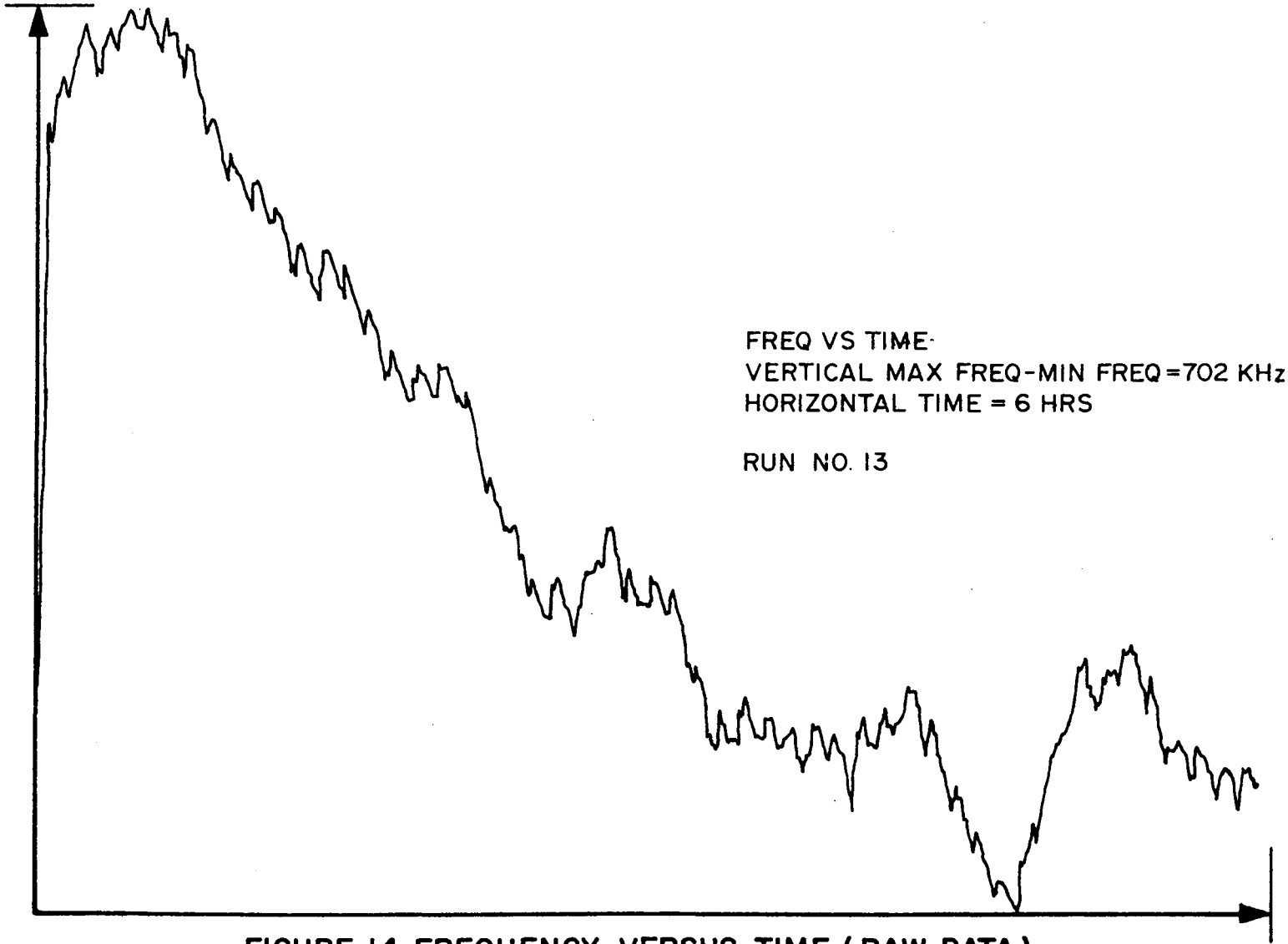

FIGURE 14 FREQUENCY VERSUS TIME (RAW DATA)

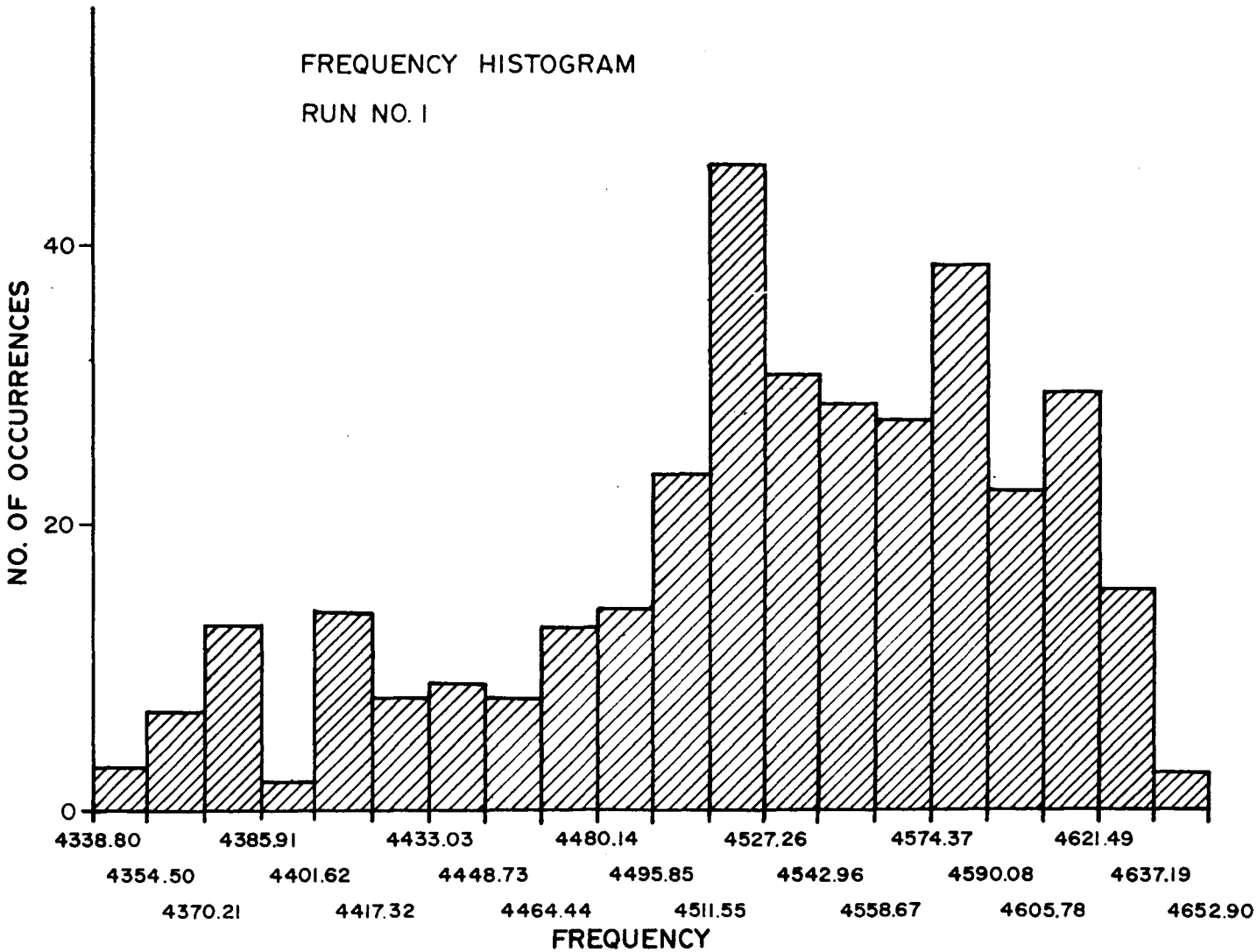

FIGURE 15 FREQUENCY HISTOGRAM OF RAW DATA

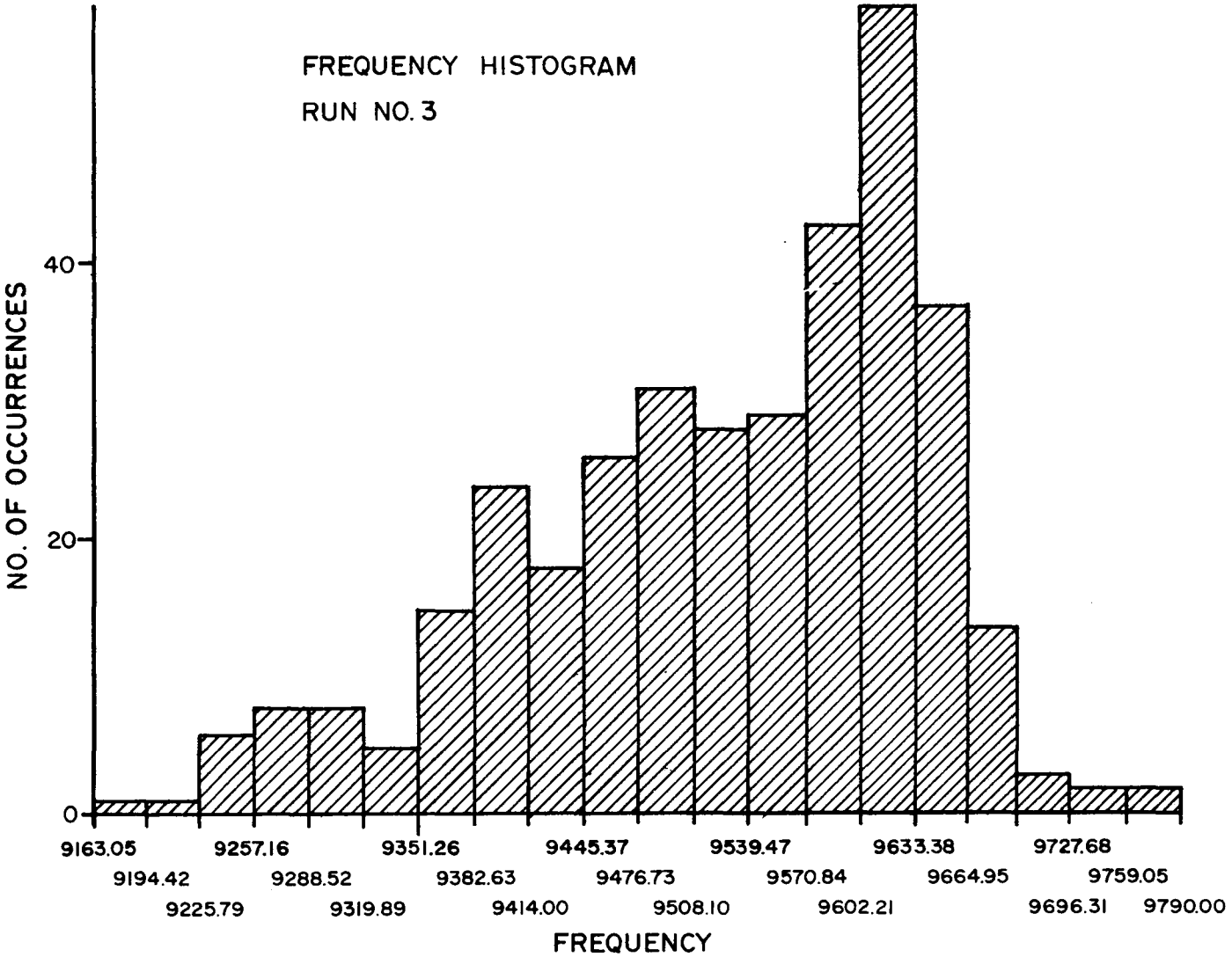

FIGURE 16 FREQUENCY HISTOGRAM OF RAW DATA

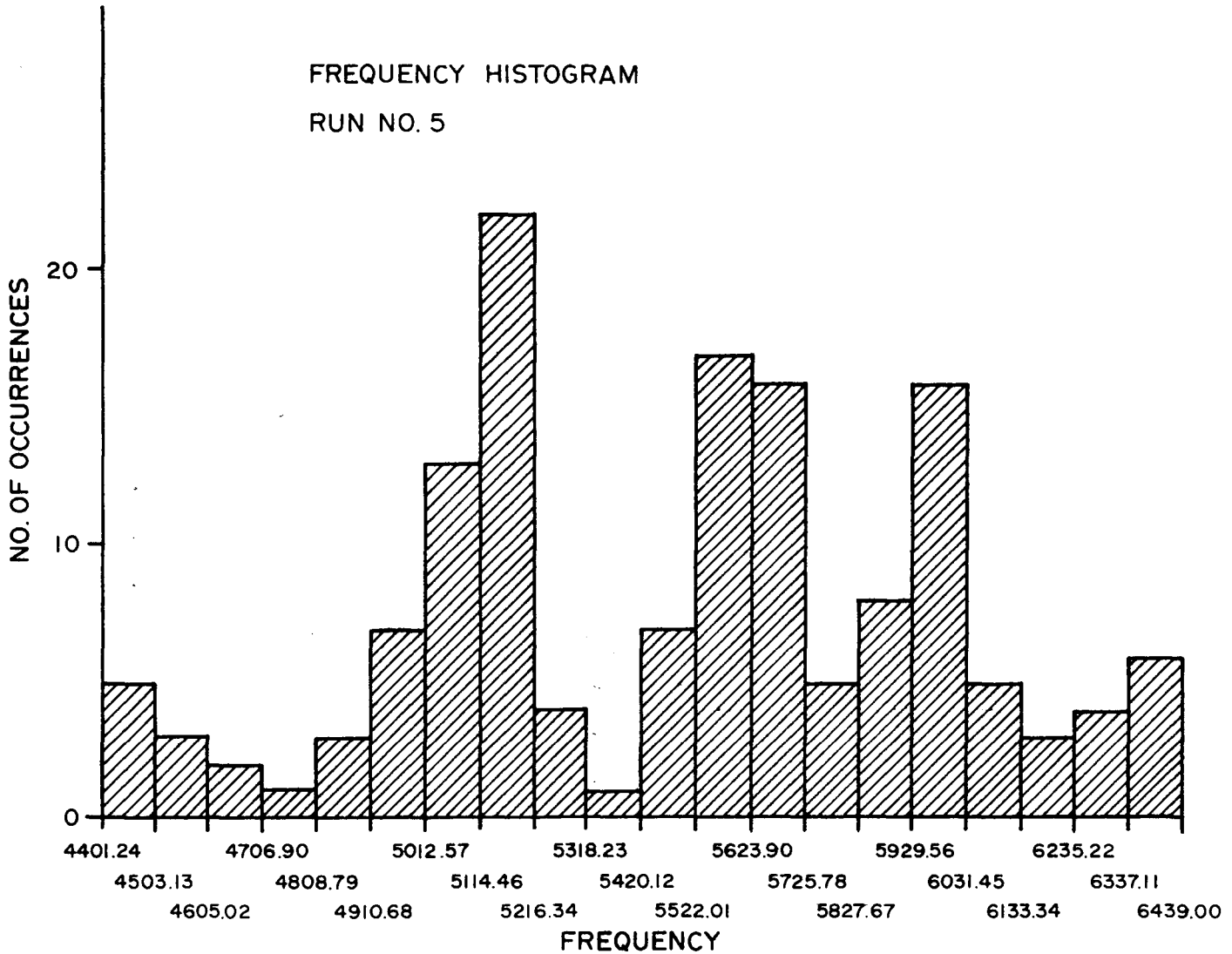

FIGURE 17 FREQUENCY HISTOGRAM OF RAW DATA

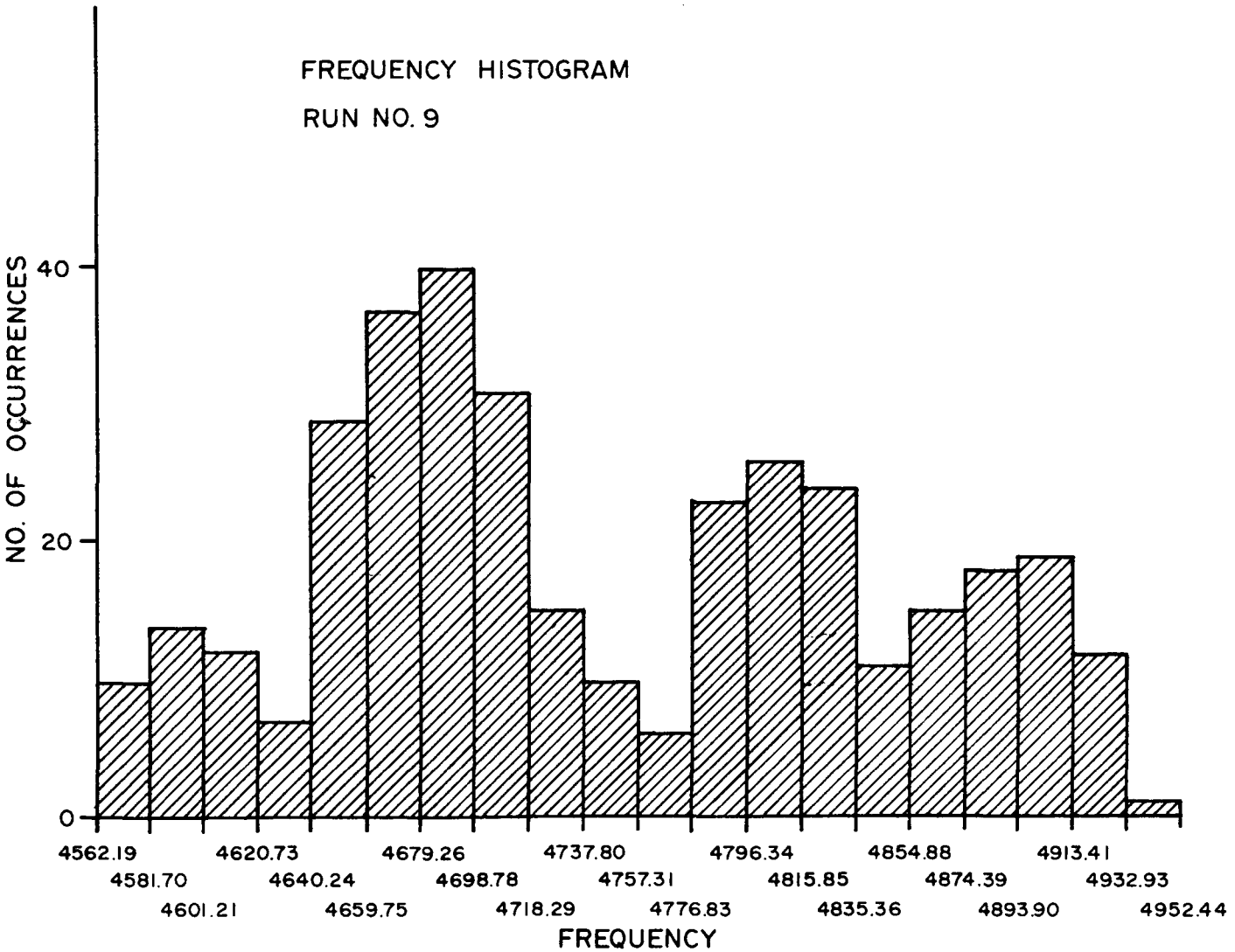

FIGURE 18 FREQUENCY HISTOGRAM OF RAW DATA

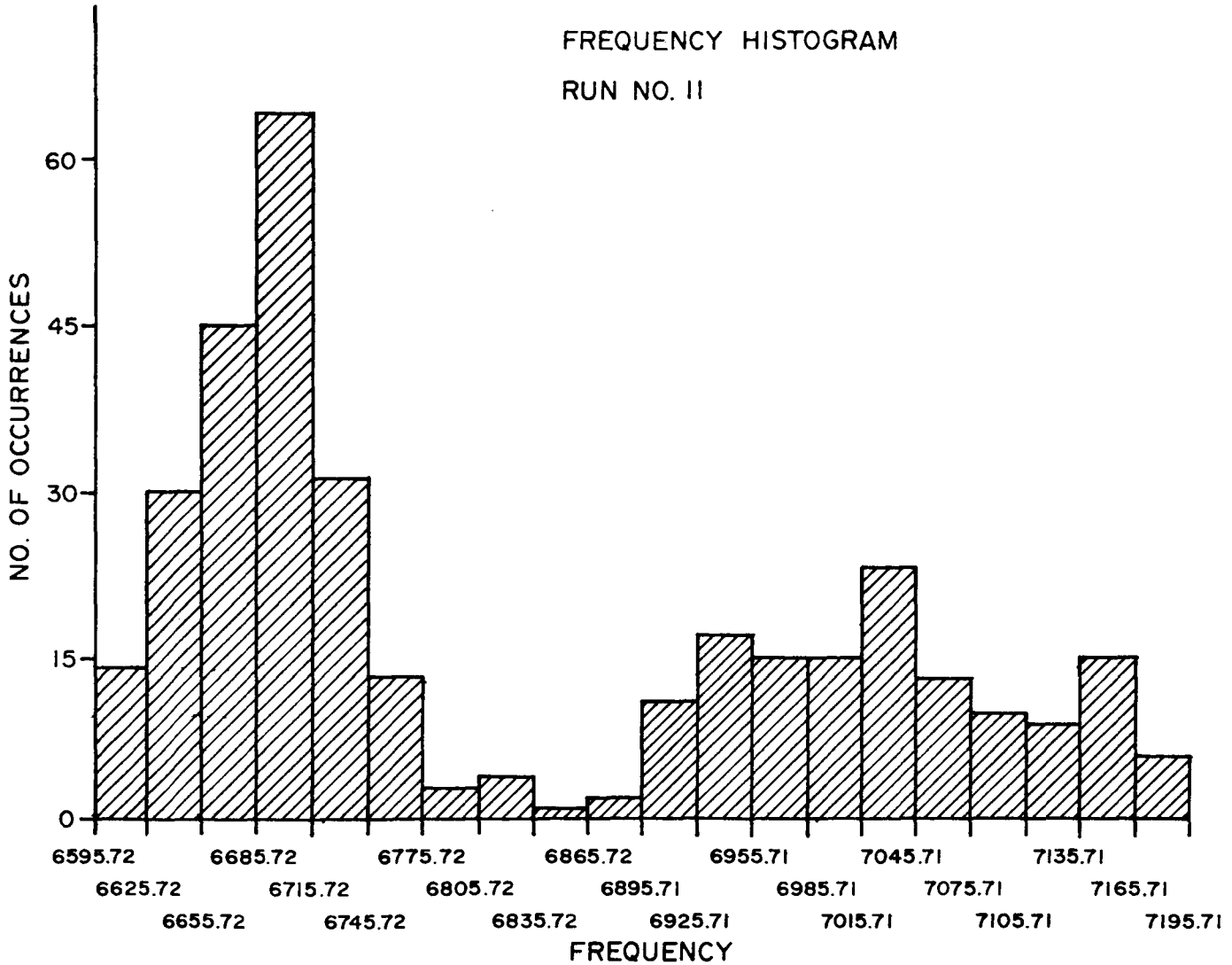

FIGURE 19 FREQUENCY HISTOGRAM OF RAW DATA

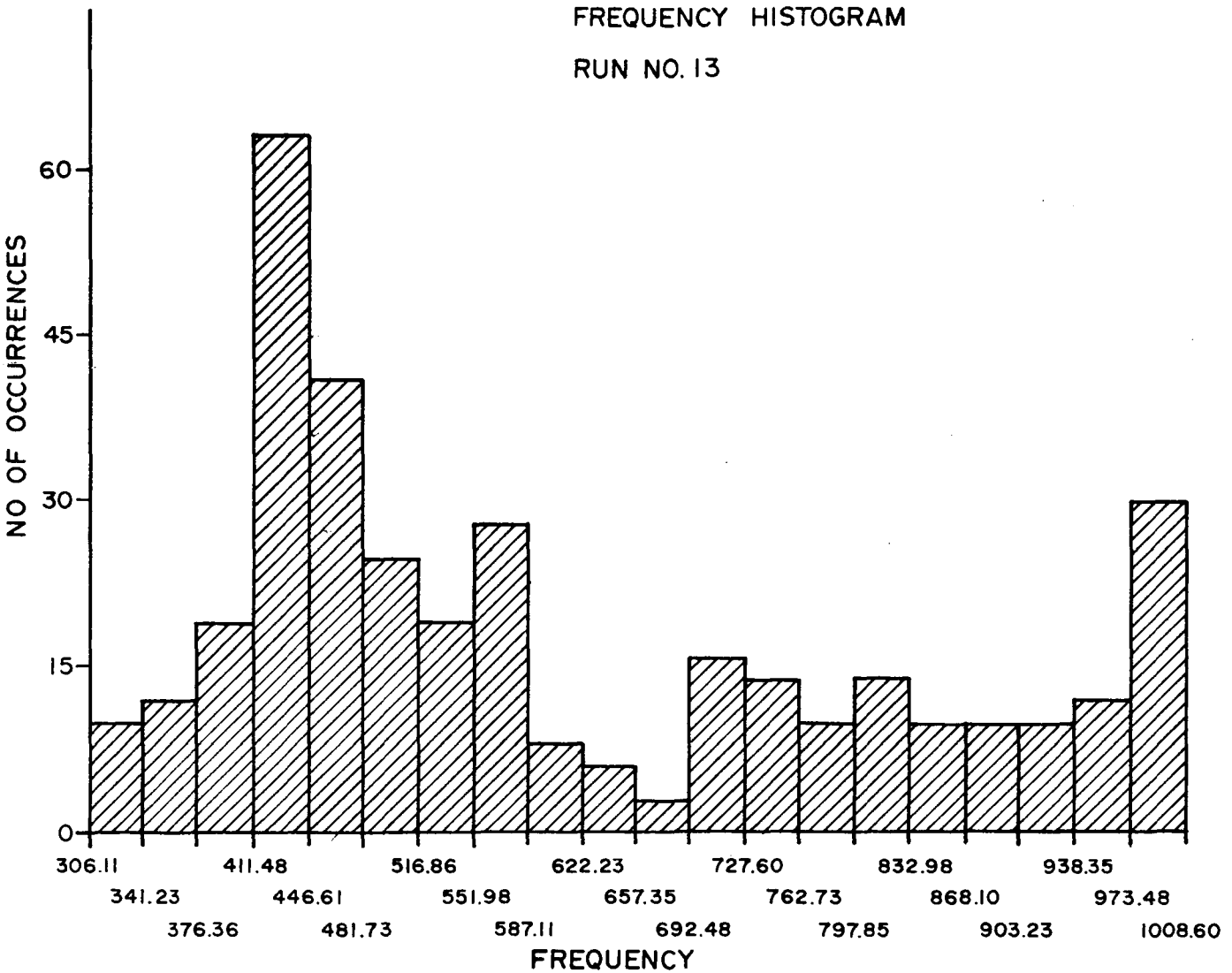

FIGURE 20 FREQUENCY HISTOGRAM OF RAW DATA

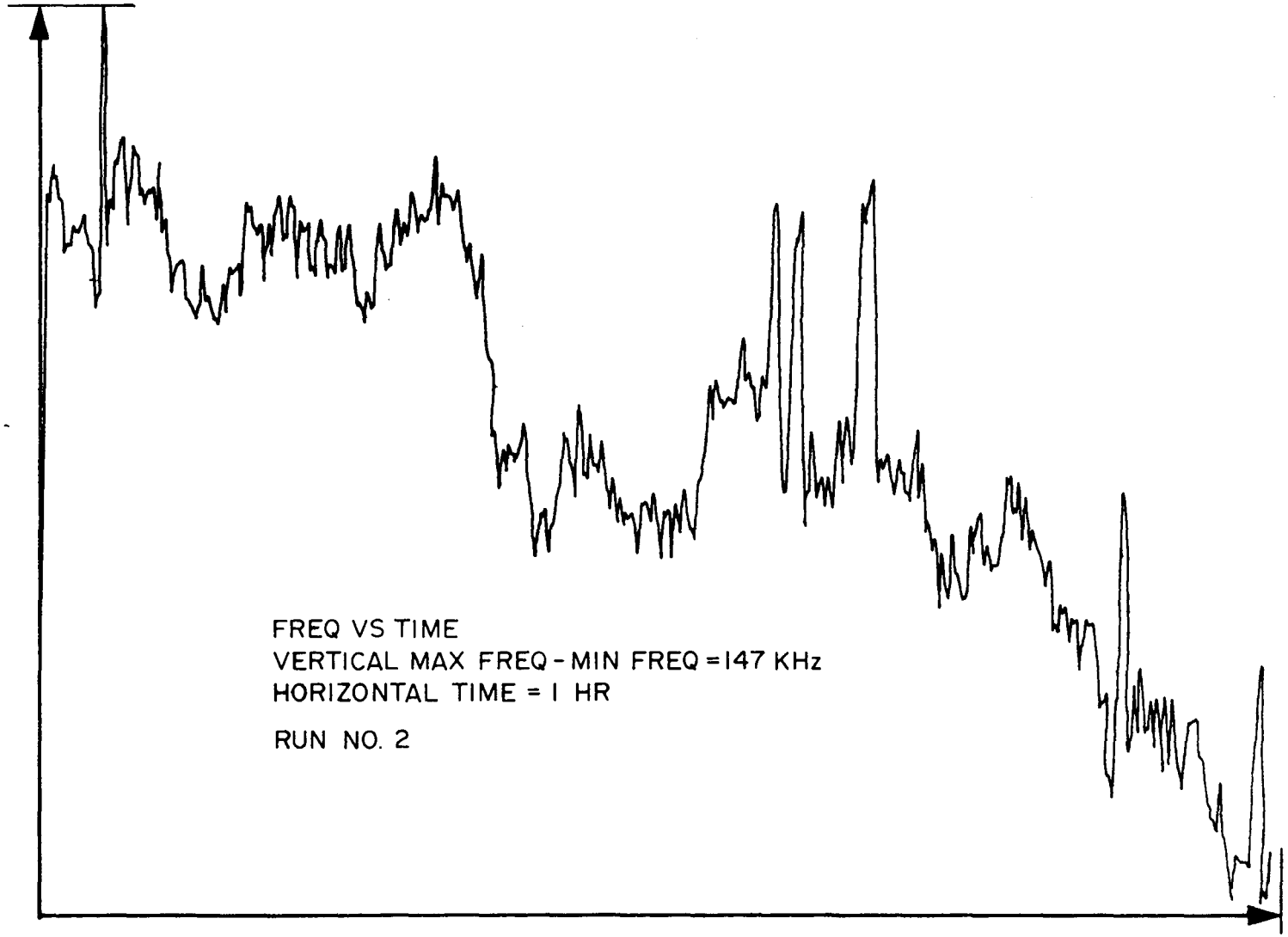

FIGURE 21 FREQUENCY VERSUS TIME (RAW DATA)

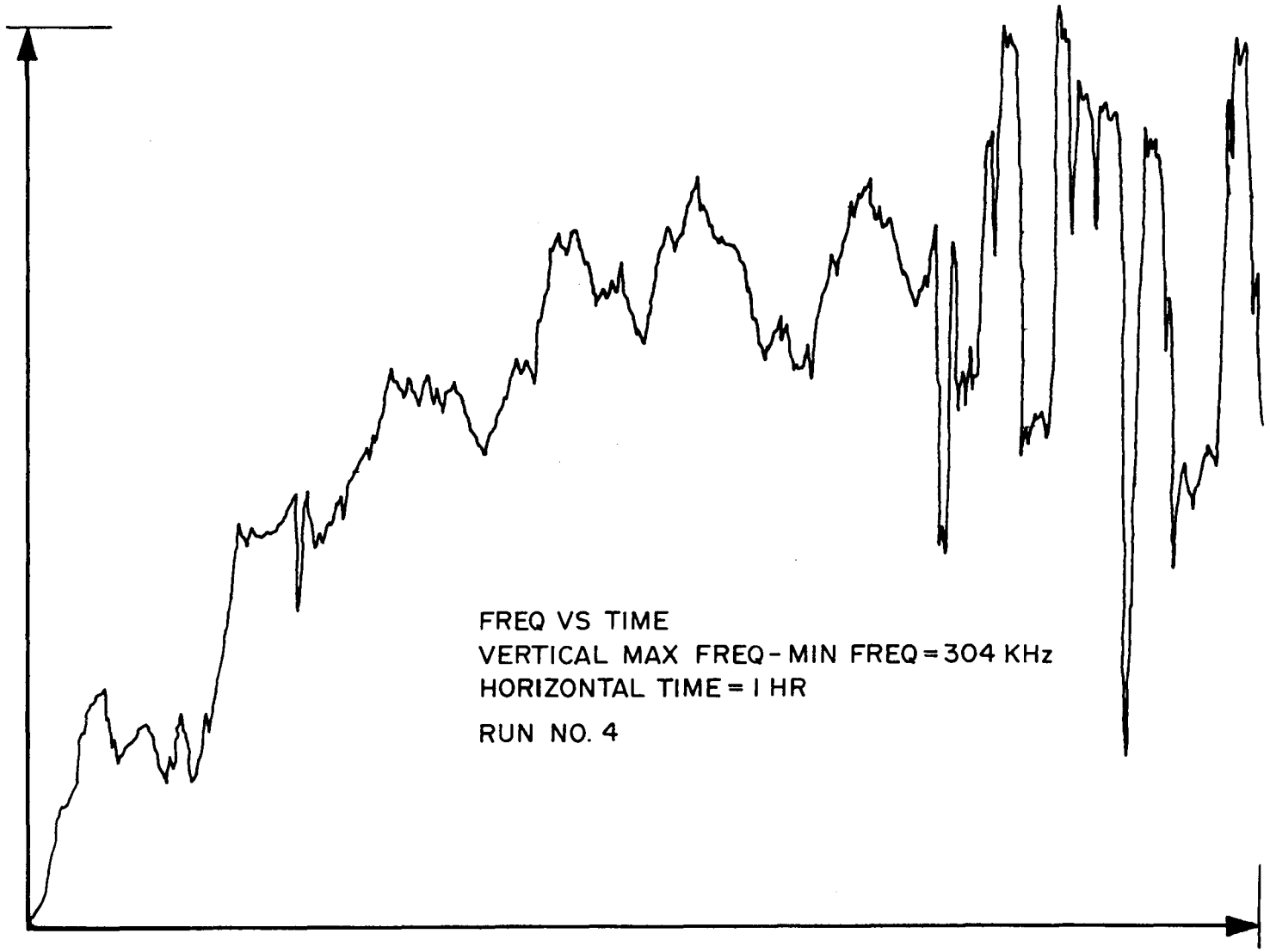

FIGURE 22 FREQUENCY VERSUS TIME (RAW DATA)

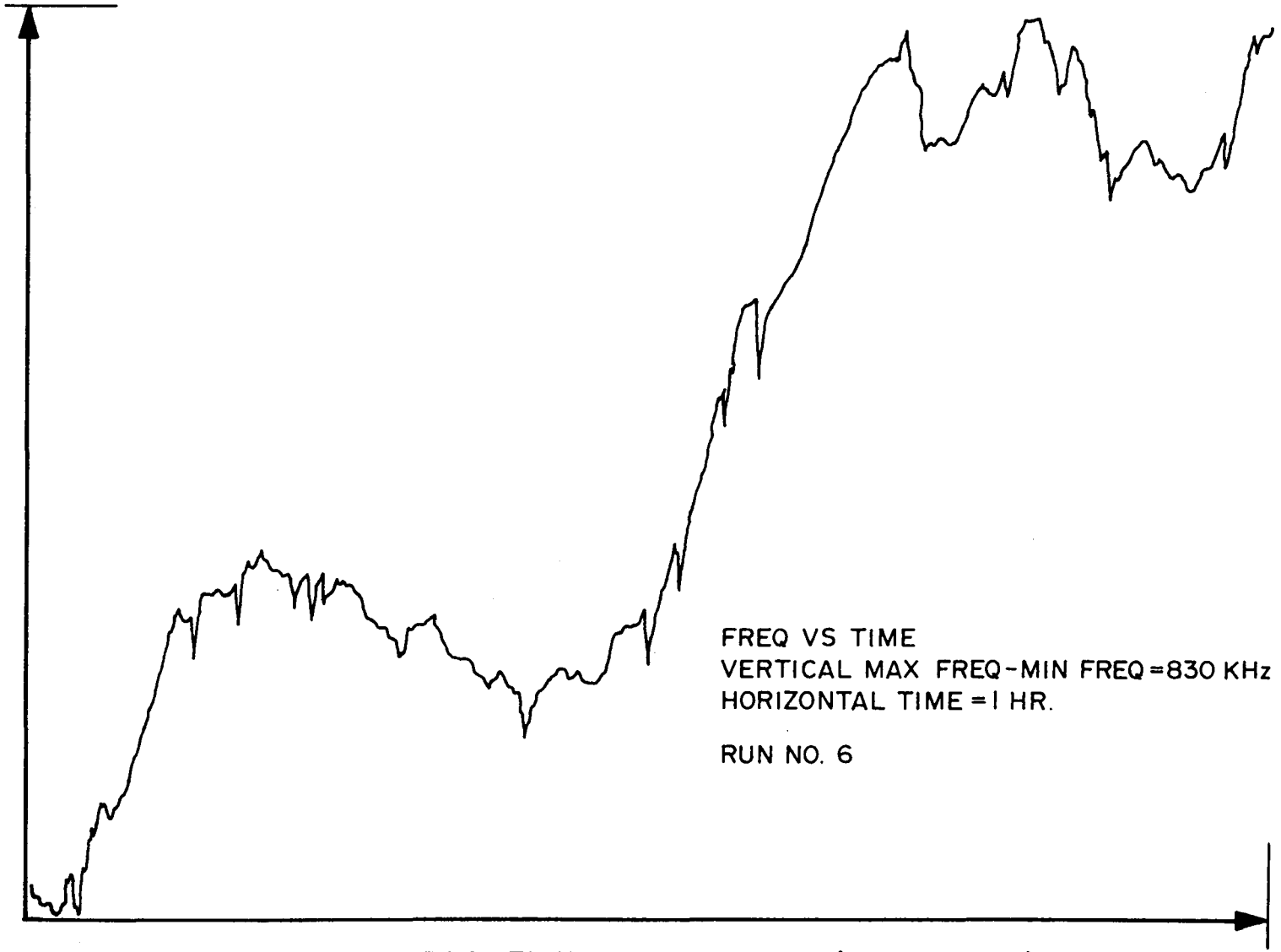

FIGURE 23 FREQUENCY VERSUS TIME (RAW DATA)

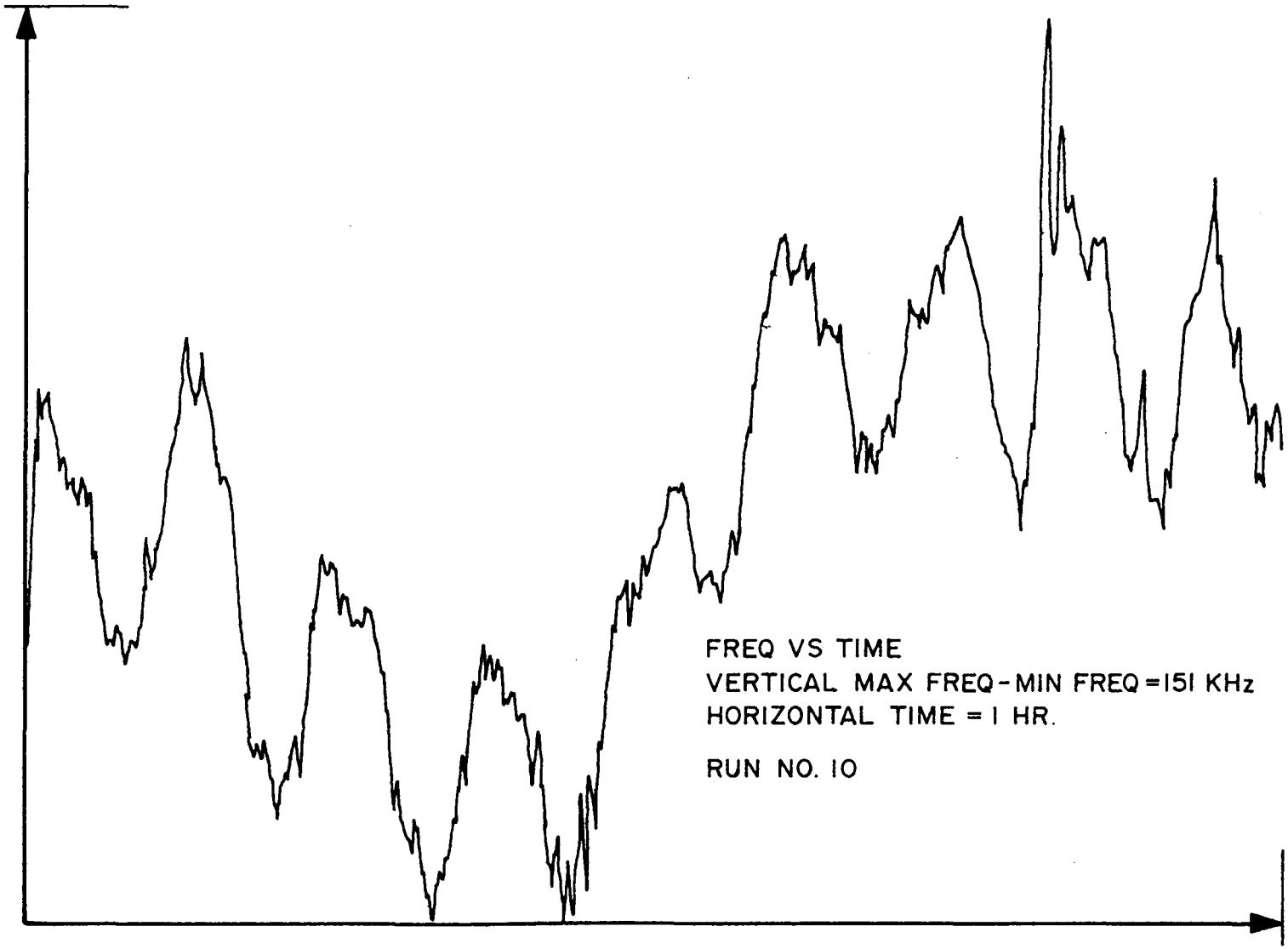

FIGURE 24 FREQUENCY VERSUS TIME (RAW DATA)

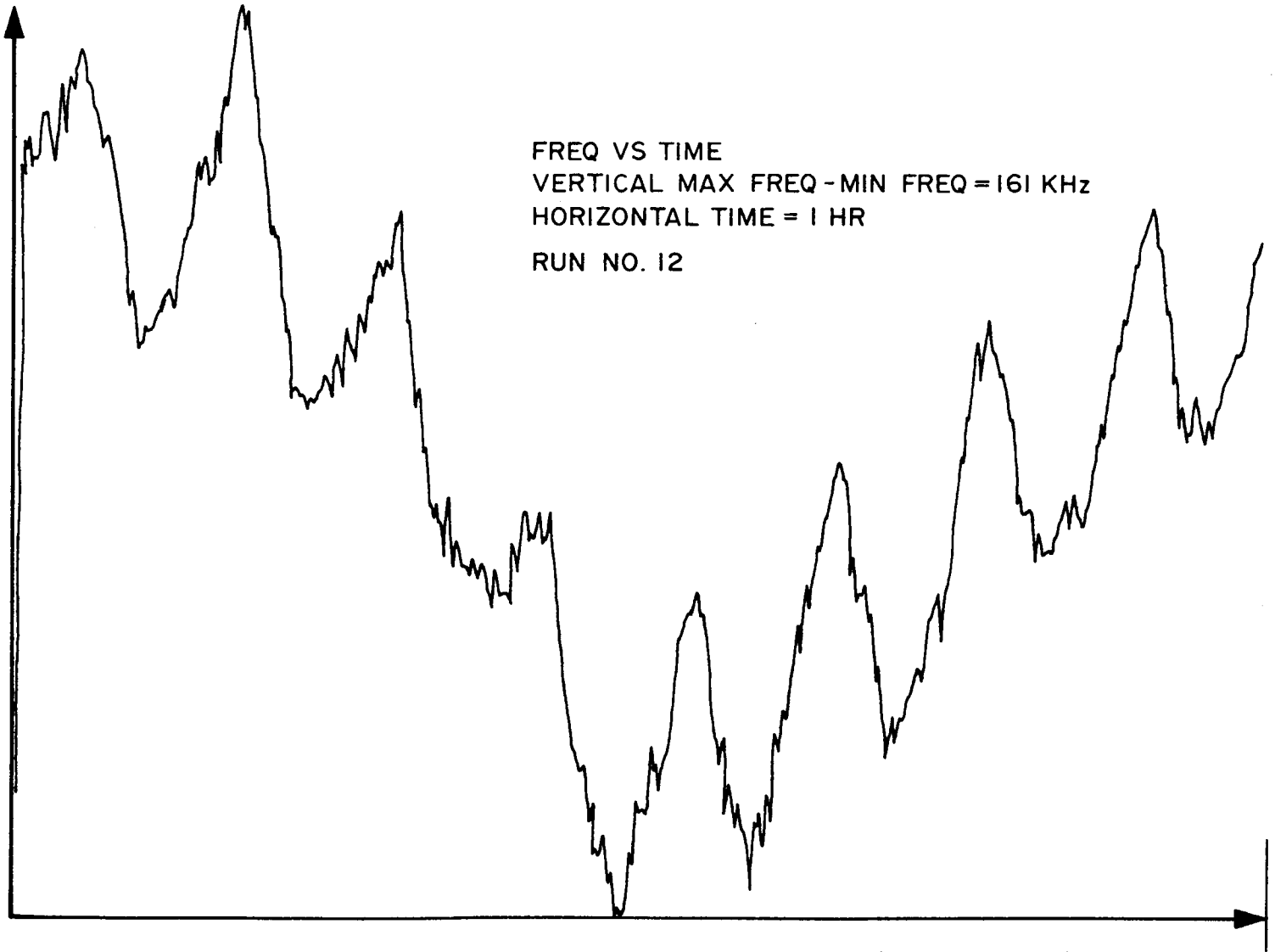

FIGURE 25 FREQUENCY VERSUS TIME (RAW DATA)

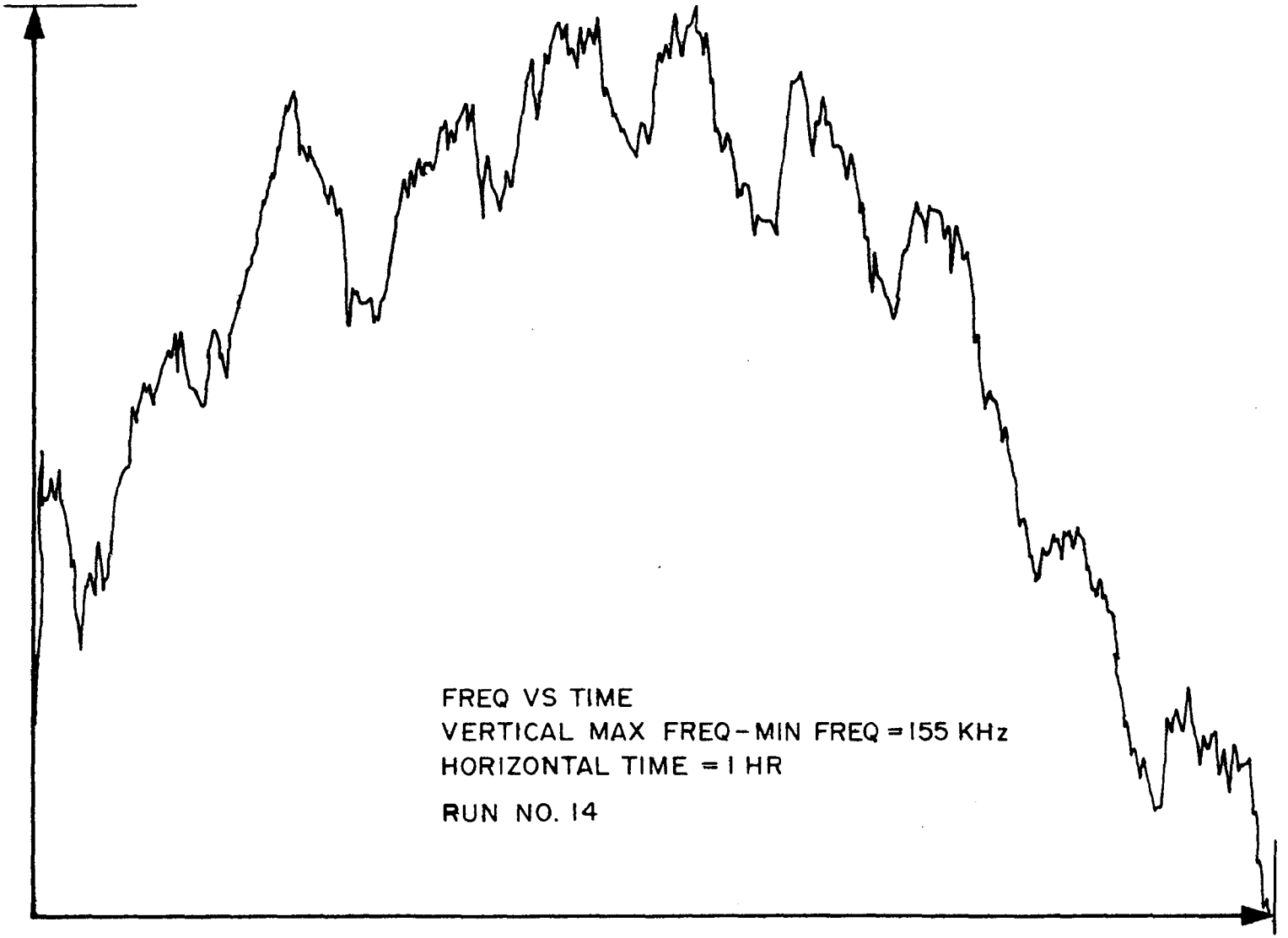

FIGURE 26 FREQUENCY VERSUS TIME (RAW DATA)

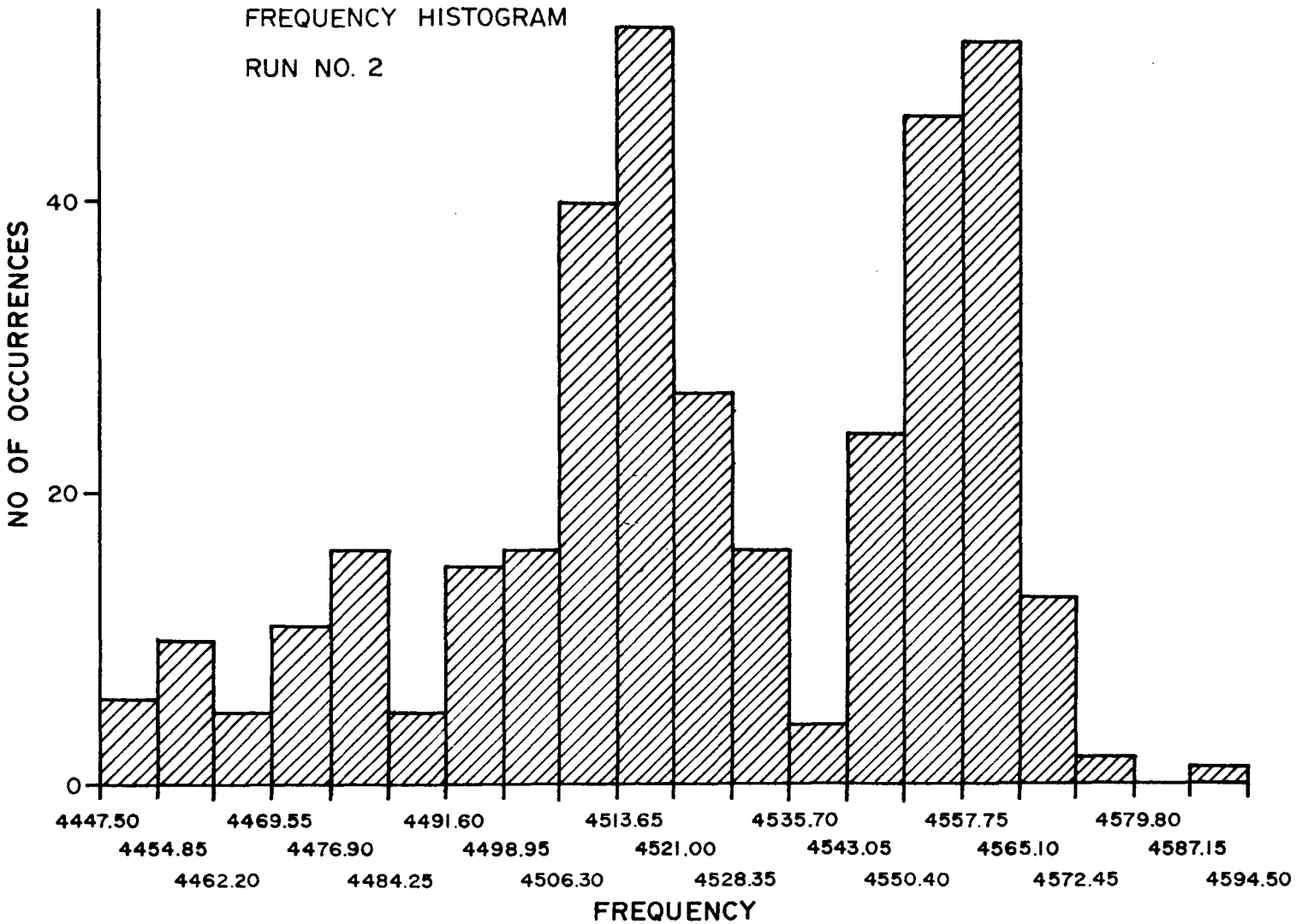

FIGURE 27 FREQUENCY HISTOGRAM OF RAW DATA

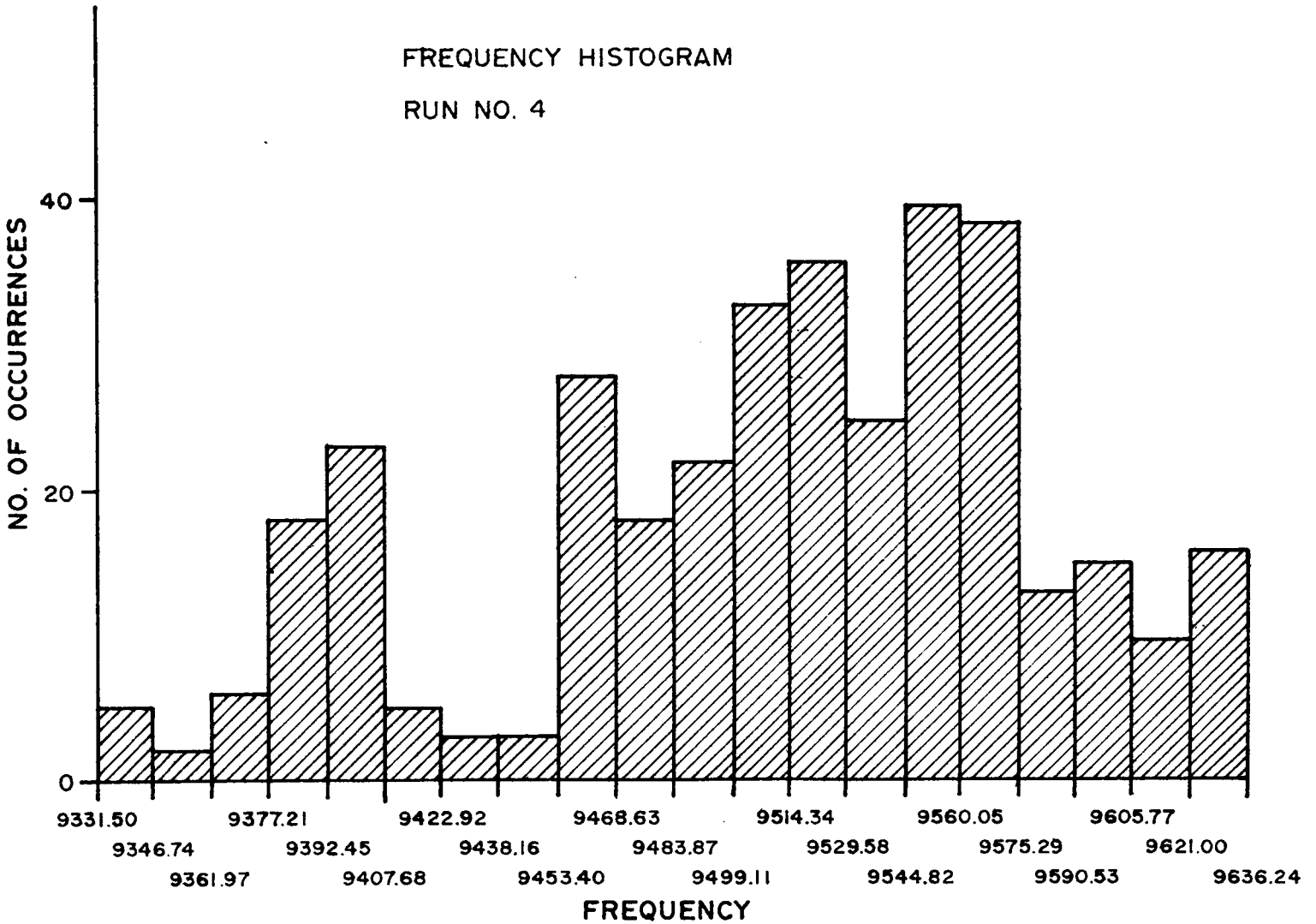

FIGURE 28 FREQUENCY HISTOGRAM OF RAW DATA

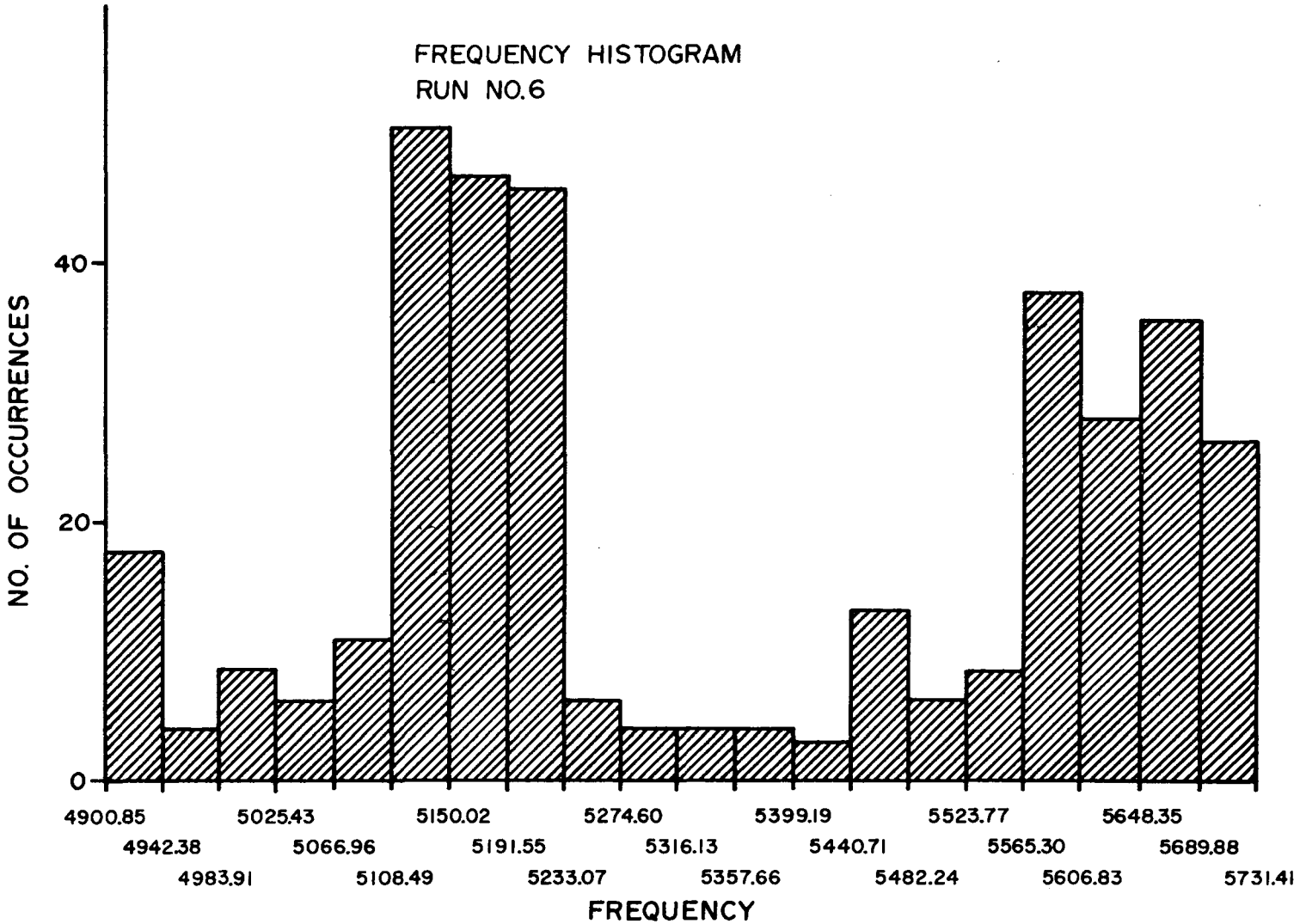

FIGURE 29 FREQUENCY HISTOGRAM OF RAW DATA

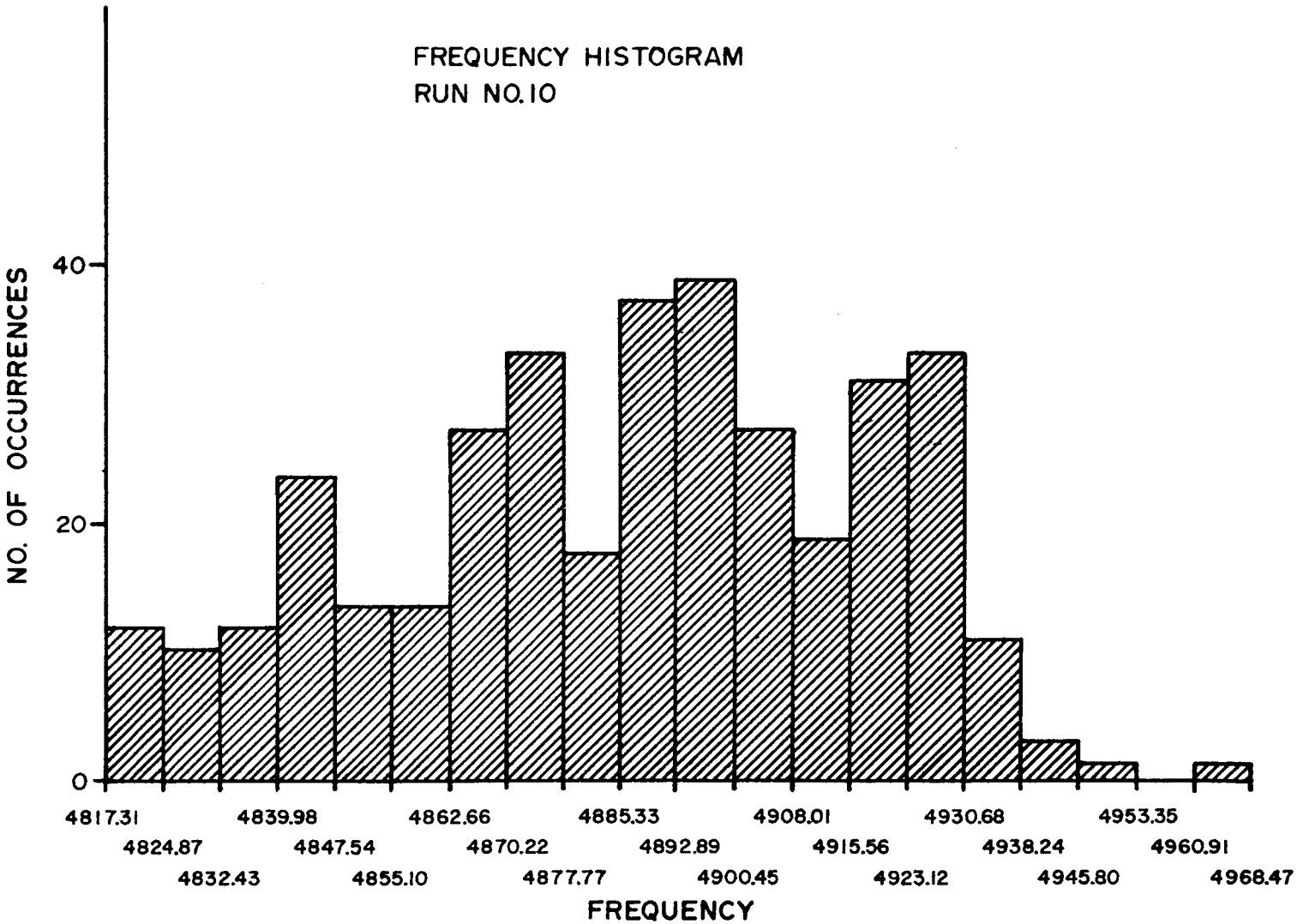

FIGURE 30 FREQUENCY HISTOGRAM OF RAW DATA

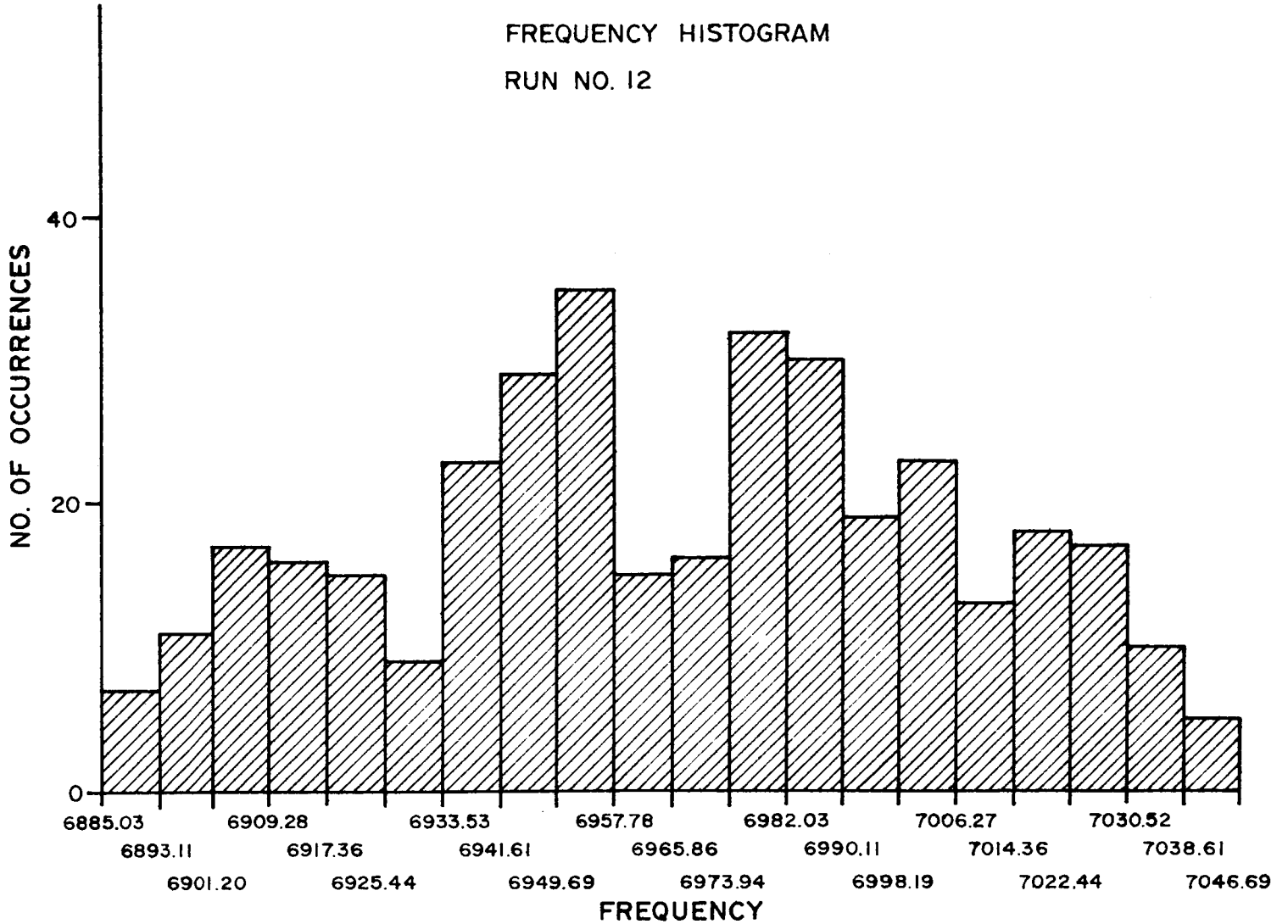

FIGURE 31 FREQUENCY HISTOGRAM OF RAW DATA

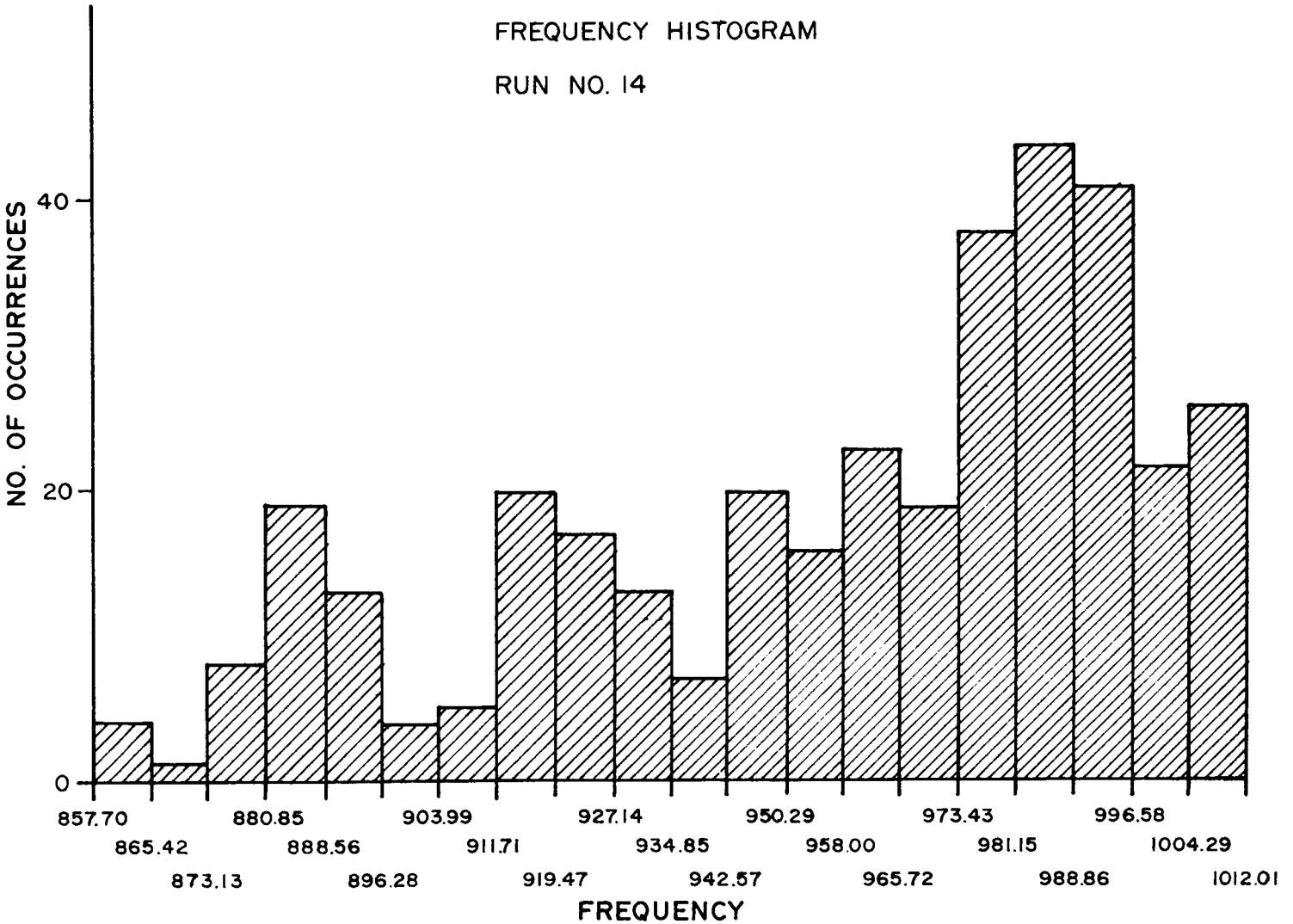

FIGURE 32 FREQUENCY HISTOGRAM OF RAW DATA

VIII. BIBLIOGRAPHY

1. Baird, K.M., Smith, D.S., Hanes, G.R., and Tsunekane, "Characteristics of a Simple Single-Mode He-Ne Laser," Applied Optics, No. 5, Vol. 4, pp. 569-571, May 1965.

2. Bennett, W.R., Jr., Jacobs, S.F., LaTourrette, J.T., and Rabinowitz, P., "Dispersion Characteristics and Frequency Stabilization of an He-Ne Gas Laser," Applied Physics Letters, No. 3, Vol. 5, pp. 56-58, August 1, 1964.

3. Jaseja, T.S., Javan, A., and Townes, C.H., "Frequency Stability of He-Ne Masers and Measurements of Length," Physical Review Letters, No. 5, Vol. 10, pp. 165-167, March 1, 1963.

4. Collinson, J.A., "A Stable, Single-Frequency RF-Excited Gas Laser at 6328Å," The Bell System Technical Journal, pp. 1511-1519, September 1965.

5. DiDomenico, M., Jr., "Characteristics of a Single-Frequency Michelson-Type He-Ne Gas Laser," IEEE Journal of Quantum Electronics, No. 8, Vol. QE-2, pp. 311-322, August 1966.

6. Goldich, H D., "Frequency Stabilization of Double-Mode Gas Laser," IEEE Proceedings, p. 638, June 1965.

7. Javan, A., Bollik, E.A., and Bond, W.L., "Frequency Characteristics of a Continuous Wave He-Ne Optical Maser," Journal of the Optical Society of America, No. 1, Vol. 52, pp. 96-98, January 1962.

8. Lipsett, Morley S. and Lee, Paul H., "Laser Wavelength Stabilization with a Passive Interferometer," Applied Optics, No. 5, Vol. 5, p. 823, May 1966.

9. Mielenz, K.D., Stephens, R.B., Gillilland, K.E., and Nefflen, K.F., Measurement of Absolute Wavelength Stability of Lasers," Optical Society of America Journal, No. 2, Vol. 56, pp. 156-162, February 1966.

10. Muldoon, H , Bicevskis, I., and Steele, A., "Stabilized Gas Laser Oscillators," Final Report, NASA Contract No. NAS5-3927, Goddard Space Flight Center, Greenbelt, Maryland, Accession No. N67-14893, June 1966.

11. Polanyi, T.G., Skolnick, M.L., and Tobias, I., "Frequency Stabilization of a Gas Laser," IEEE Journal of Quantum Electronics, p. 178, July 1966.

12. Rabinowitz, P. and LaTourrette, J.T., "Frequency Stabilized Gas Lasers," Phase I Study Report, NASA Contract No. NAS8-11773, Geo. C. Marshall Space Flight Center, Huntsville, Alabama, Accession No. N65-31013, July 1965.

13. Reynolds, R.S., Foster, J.D., Kamiya, A.A., and Siegman, A.E., "Frequency Stabilized Gas Lasers," Final Report, NASA Contract No. NAS8-20631, Geo. C. Marshall Space Flight Center, Huntsville, Alabama, Accession No. N67-20379, February 1967.

14. Shimoda, Koichi, and Javan, Ali, "Stabilization of the He-Ne Maser on the Atomic Line Center," Journal of Applied Physics, Vol. 36, pp. 718-726, March 1965.

15. Shimoda, Koichi, "Frequency Stabilization of the He-Ne Maser," IEEE Transactions on Instrumentation and Measurement, pp. 170-174, December 1964.

16. Smith, P.W., "Stabilized, Single-Frequency Output from a Long Laser Cavity," IEEE Journal of Quantum Electronics, No. 8, Vol. QE-1, November 1965.

17. Smith, P.W., "On the Stabilization of a High-Power Single-Frequency Laser," IEEE Journal of Quantum Electronics, No. 9, Vol. QE-2, pp. 666-668, September 1966.

18. Hsi-ming, Ten, Jun-Wen, Wang, and Chen-li, Hsia, "The Formation Time of Optical Oscillation of Laser," K'O-hsueh T'ung-pao (issuing agency), Accession No. N66-15050, October 1965.

19. Tobias, Irwin, Skolnick, Michael L., Wallace, Robert A., and Polanyi, Thomas G., "Derivation of a Frequency-Sensitive Signal from a Gas Laser in an Axial Magnetic Field," Applied Physics Letters, No. 10, Vol. 6, p. 198, May 1965.

20. White, A.D., "Frequency Stabilization of Gas Lasers," IEEE Journal of Quantum Electronics, No. 8, Vol. QE-1, pp. 349-357, November 1965.

21. White, A.D., Gordon, E.I., and Labuda, E.F., "Frequency Stabilization on Single Mode Gas Lasers," Applied Physics Letters, No. 5, Vol. 5, pp. 97-98, September 1, 1964.

The vita has been removed from the scanned document

X. APPENDIX

Off Axis Reference Cavity

Because of its complexity and scope, no attempt will be made to present a detailed analysis of the theory of optical resonators in general. However, characteristics of the optical resonator used in this system will be discussed. The resonance condition necessary to establish an interlaced mode pattern within the passive resonator cavity will be discussed in terms of the geometry of the cavity. With the resonance condition as a constraint the reflection conditions will be discussed and pertinent equations derived. These equations are necessary to specify a small length, ϵ, one of the cavity parameters. This length, ϵ, in conjunction with the mirror radius, R, specifies the mirror separation for the cavity. From the general theory of resonators, a true confocal resonator (mirrors of equal radius separated by the length of one radius) represents a barely stable condition, since, if the two mirrors have the slightest difference of curvature the confocal configuration becomes unstable with regards to diffraction losses. Stable configuration can be restored by making the separation of the two mirrors slightly shorter than the length of the radius of either of the equal radius mirrors, herein lies the importance of the previously mentioned length ϵ.

The optical resonator used in this system is considered a near confocal situation since the mirror separation is $R + \epsilon$ (where ϵ is negative in practice). The resonator is also considered a circulating resonator, which means no reflected light is returned directly along the incident beam. The advantage offered is the avoidance of wavelength pulling caused by spurious reflections. This condition of circulating resonator

is accomplished by illuminating a spherical mirror cavity off axis. This condition is shown in figure A-1.

The cavity is comprised by two identical spherical mirrors, M_1 and M_2, at a near confocal spacing of $R + \epsilon$ (ϵ is negative in practice). When the rays retrace themselves over a pathlength having an integral number of wavelengths they return on themselves in phase and an interlaced mode pattern is set up, evidence by two bright spots on mirror M_2, and two bright lines on mirror M_1. When the wavelength of the incident beam changes from λ to $\lambda + \Delta\lambda$, the spots on mirror M_2 remain stationary but the lines on mirror M_1 move apart or together, dependent on the sign of the change $\Delta\lambda$. As an aid to visualizing the process only, one may think of the light spots on mirror M_2 as a pivot point and of the beam from mirror M_1 to mirror M_2 as a lever extending past mirror M_2 through the light spot on M_2; then it becomes obvious that as the lines on M_1 move apart or together, the transmitted beam (analogous lever extension past M_2) undergoes an angle change, θ, which is a function of the motion of the lines of mirror M_1, which in turn is a function of the wavelength change $\Delta\lambda$. Therefore the angle of the transmitted beam becomes an extremely sensitive function of wavelength. This effect is the basis of an optical discriminator. The change in angle of the transmitted beam, with motion of the lines on M_1, is shown in figure A-2. From the changes in angle of the transmitted beam an analog electric signal is obtained which varies with $\Delta\lambda/\lambda$. This signal is amplified and applied to a piezoelectric transducer which controls the mirror spacing of the laser source.

From the use of the ray diagrams of figure A-3 we are able to derive the expression for the resonance condition of the near confocal cavity

arrangement. The back surfaces of the identical spherical mirrors are curved to function as a positive lens which focuses an incident parallel beam at P_1 on M_1 to P_2 on the far mirror M_2. All rays of the diagram are considered in the same horizontal plane. A beam is incident off axis at P_1 on M_1 and illuminates a patch of diameter d. This beam is focused to a point at P_2 on M_2 where it undergoes a reflection to P_3, P_4 and on to P_5, near P_1 on M_1. The optical pathlength traversed in going from P_1 to P_2 is denoted by ℓ_1, likewise for the subsequent pathlengths ℓ_2, ℓ_3, and ℓ_4. The total pathlength, L, then is

$$L = \ell_1 + \ell_2 + \ell_3 + \ell_4$$

An axis for the system is defined by a line connecting the centers of curvature of the two mirrors. The distances Y_1, Y_2, Y_3, Y_4, Y_5 are the normal distances of the respective points P_1, P_2, P_3, P_4, P_5 from the axis.

The resonance condition for the observed mode distribution requires that:

1. P_5 coincide with P_1

therefore $Y_3 = Y_5$

2. The axis be a line of symmetry

therefore $Y_1 = Y_3 = Y_5$

$Y_2 = Y_4$

$\ell_1 + \ell_2 = \ell_3 + \ell_4$

3. The total optical pathlength be an integral number of wavelengths.

therefore

$$L = \ell_1 + \ell_2 + \ell_3 + \ell_4 = 2(\ell_1 + \ell_2)$$

and

$$N \lambda = 2(\ell_1 + \ell_2) \tag{1}$$

to satisfy the requirement of the resonance condition then we need to calculate ℓ_1 and ℓ_2. From figure A-3:

$$\ell_1^2 = a^2 + (Y_1 - Y_2)^2 \tag{2}$$

and

$$R + \epsilon = a + c + d \tag{3}$$

or

$$a = R + \epsilon - c - d \tag{4}$$

since the radius of mirror M_2 is the perpendicular bisector of the chord $P_2 P_4$, and since $Y_2 = Y_4$ we have

$$Y_2^2 = (2R - d)\, d \tag{5}$$

On transposing and applying the quadratic formula to equation (5) we obtain

$$d = R - \left[R^2 - Y_2^2 \right]^{1/2} \tag{6}$$

Now since the radius of mirror M_1 is the perpendicular bisector of chord $P_1 P_3$, we have for c

$$c = R - \left[R^2 - Y_1^2 \right]^{1/2} \tag{7}$$

Substitution of equations (6) and (7) into (4) produces

$$a = (\epsilon - R) + \left[(R^2 - Y_1^2)^{1/2} + (R^2 - Y_2^2)^{1/2} \right] \tag{8}$$

and

$$a^2 = (\epsilon - R)^2 + 2(\epsilon - R) \left[(R^2 - Y_1^2)^{1/2} + (R^2 - Y_2^2)^{1/2} \right]$$

$$+ \left[(R^2 - Y_1^2)^{1/2} + (R^2 - Y_2^2)^{1/2} \right]^2 \tag{9}$$

which on expanding becomes:

$$a^2 = 3R^2 + \epsilon^2 - 2\epsilon R - (Y_1^2 + Y_2^2)$$

$$+ 2R (\epsilon - R) \left[(1 - Y_1^2/R^2)^{1/2} + (1 - Y_2^2/R^2)^{1/2} \right] \tag{10}$$

$$+ 2R^2 \left[(1 - Y_1^2/R^2) \ (1 - Y_2^2/R^2) \right]^{1/2}$$

recalling equation (2) and substituting (10),

$$\ell_1^2 = 3R^2 + \epsilon^2 - 2\epsilon R - 2\, Y_1\, Y_2$$

$$+ 2R\,(\epsilon - R)\left[\,(1 - {Y_1^2}/{R^2})^{1/2} + (1 - {Y_2^2}/{R^2})^{1/2}\,\right]$$

$$+ 2R^2\left[\,(1 - {Y_1^2}/{R^2})\,(1 - {Y_2^2}/{R^2})\,\right]^{1/2} \qquad (11)$$

We make the following substitutions for simplicity:

$$\alpha = 3R^2 + \epsilon^2 - 2\epsilon R + 2R\,(\epsilon - R)\left[(1 - {Y_1^2}/{R^2})^{1/2} + (1 - {Y_2^2}/{R^2})^{1/2}\right]$$

$$+ 2R^2\left[(1 - {Y_1^2}/{R^2})\,(1 - {Y_2^2}/{R^2})\,\right]^{1/2}$$

$$\beta = \left[1 - {Y_1^2}/{R^2}\,\right]^{1/2}$$

$$\gamma = \left[1 - {Y_2^2}/{R^2}\,\right]^{1/2}$$

$$\delta = 2\, Y_1\, Y_2$$

then equation (11) becomes

$$\ell_1^2 = \alpha - \delta \qquad (12)$$

So with the exact same approach as for ℓ_1^2 we obtain:

$$\ell_2^2 = \alpha + \delta \tag{13}$$

From expressions (12), (13), and (1) we have for the resonance condition

$$N \lambda = 2 \left[(\alpha + \delta)^{1/2} + (\alpha - \delta)^{1/2} \right] = L \tag{14}$$

Where L is the total optical path and α and δ are the substitutions made earlier.

The resonance condition just derived imposes certain geometrical restraints on the reflection characteristics of this cavity. Satisfying the equations corresponding to resonance do not in general satisfy the conditions of reflection. For a given parallel ray and spherical mirror of radius, R, there exists some mirror displacement, hence an ϵ for which that parallel ray retraces itself and satisfies the resonance condition. From figure A-4 we may calculate the geometrical relationships.

$$\text{Sin } \alpha = Y/R \tag{15}$$

$$\text{Cos } \beta = X \left[(2\ Y)^2 + X^2 \right]^{-1/2} \tag{16}$$

Using the trigonometric formula for half angles

$$\text{Sin } \beta/2 = \left(\frac{1 - \text{Cos } \beta}{2} \right)^{1/2} \tag{17}$$

Since the angle of incidence must equal the angle of reflection, we may determine the parameter X, hence

$$\text{Sin } \alpha = \text{Sin } \beta/2 \tag{18}$$

and

$$\frac{Y}{R} = \left(1 - \frac{X}{\left[4Y^2 + X^2\right]^{1/2}}\right)^{1/2}$$

squaring, transposing and cancelling we obtain

$$X = 2\,\frac{(R^2 - Y^2)}{\left[2R^2 - Y^2\right]^{1/2}} \tag{19}$$

From figure A-5 we may derive an expression for the value of ϵ commensurate with the other cavity parameters. From triangle ABC:

$$P = (R^2 - Y^2)^{1/2} \tag{20}$$

also

$$P + a = X \tag{21}$$

and

$$\epsilon = a + b \tag{22}$$

substitution of (22) into (21) gives

$$b = P + \epsilon - X \tag{23}$$

Again from the figure

$$\frac{R}{2} + \left(\frac{R}{2} - b\right) = P \tag{24}$$

substitution of (23) and (20) into (24) produces

$$\epsilon = R + X - 2(R^2 - Y^2)^{1/2} \tag{25}$$

Hence a further condition is imposed by the reflection angles and constrains the value of ϵ. The value of X in equation (25) for ϵ is given by equation (19).

On satisfying these conditions of reflection we are able to specify an angle θ mentioned previously as the angle associated with the transmitted beam, which is the same as angle α of figure A-4, i.e.,

$$\text{Sin } \alpha = \text{Sin } \beta/2 = \text{Sin } \theta \tag{26}$$

This angle is an extremely sensitive function of wavelength change and therefore of wavelength. A quantity $d\theta/d\lambda$ may be specified which shows the rate of change of this transmitted beam angle with change in the incident wavelength. From equation (15) and the above:

$$\text{Sin } \theta = Y_1/R \tag{27}$$

differentiating

$$\text{Cos } \theta \ \frac{d\theta}{d\lambda} = \frac{1}{R} \ \frac{dY_1}{d\lambda} \tag{28}$$

Also from $N\lambda = L$

$$\frac{dL}{dY_1} \ \frac{dY_1}{d\lambda} = N \tag{29}$$

substitution of (29) into (28) produces

$$\frac{d\theta}{d\lambda} = \frac{N}{R \dfrac{dL}{dY_1}} \tag{30}$$

We now desire $\dfrac{dL}{dY_1}$ in terms of the other cavity parameters. Using

$$L = 2 \left(\left[\alpha + \delta \right]^{1/2} + \left[\alpha - \delta \right]^{1/2} \right) \tag{31}$$

$$\alpha = 3R^2 + \epsilon^2 - 2\epsilon R + 2R (\epsilon - R) (\beta + \gamma) + 2R^2 \beta \gamma \tag{32}$$

substituting for β and γ

$$\alpha = 3R^2 + \epsilon^2 - 2\epsilon R + 2R (\epsilon - R) \left[(1 - {Y_1}^2/_{R^2})^{1/2} + (1 - {Y_2}^2/_{R^2})^{1/2} \right] \tag{33}$$

$$+ 2R^2 \ (1 - {Y_1}^2/_{R^2})^{1/2} \ \ (1 - {Y_2}^2/_{R^2})^{1/2}$$

$$\delta = 2 Y_1 Y_2 \tag{34}$$

we find

$$\frac{dL}{dY_1} = \frac{1}{(\alpha + \delta)^{1/2}} \left[\frac{\partial \alpha}{\partial Y_1} + \frac{\partial \delta}{\partial Y_1} \right] + \frac{1}{(\alpha + \delta)^{1/2}} \left[\frac{\partial \alpha}{\partial Y_1} - \frac{\alpha \delta}{\partial Y_1} \right] \tag{35}$$

On evaluating the partial derivatives

$$\frac{dL}{dY_1} = \frac{1}{(\alpha + \delta)^{1/2}}\left[\frac{2Y_2 - 2Y_1 (\epsilon - R)}{\beta R} - 2Y_1 \frac{\gamma}{\beta} \right]$$

$$+ \frac{1}{(\alpha - \delta)^{1/2}}\left[\frac{-2Y_2 - 2Y_1 (\epsilon - R)}{\beta R} - 2Y_1 \frac{\gamma}{\beta} \right] \qquad (36)$$

substitution of equation (36) into equation (30) produces the desired result.

$$\frac{d\theta}{d\lambda} = \left[\frac{1}{(\alpha + \delta)^{-1/2} \left(2Y_2 - \frac{2Y_1 (\epsilon - R)}{\beta R} - 2Y_1 \frac{\gamma}{\beta} \right)} \right.$$

$$\left. + \frac{1}{(\alpha - \delta)^{-1/2} \left(-2Y_2 - \frac{2Y_1 (\epsilon - R)}{\beta R} - 2Y_1 \frac{\gamma}{\beta} \right)} \right] \frac{N}{R} \qquad (37)$$

where: α, β, γ, and δ are as given previously.

This quantity $\frac{d\theta}{d\lambda}$ gives a measure of the sensitivity of the optical discriminator. Using a computer the Perkin-Elmer Corporation utilized the previous equation and cavity parameters to calculate an optimum value for the quantity $\frac{d\theta}{d\lambda}$ which allowed the cavity to have both retracing rays, i.e., (high Q) and good resolution.

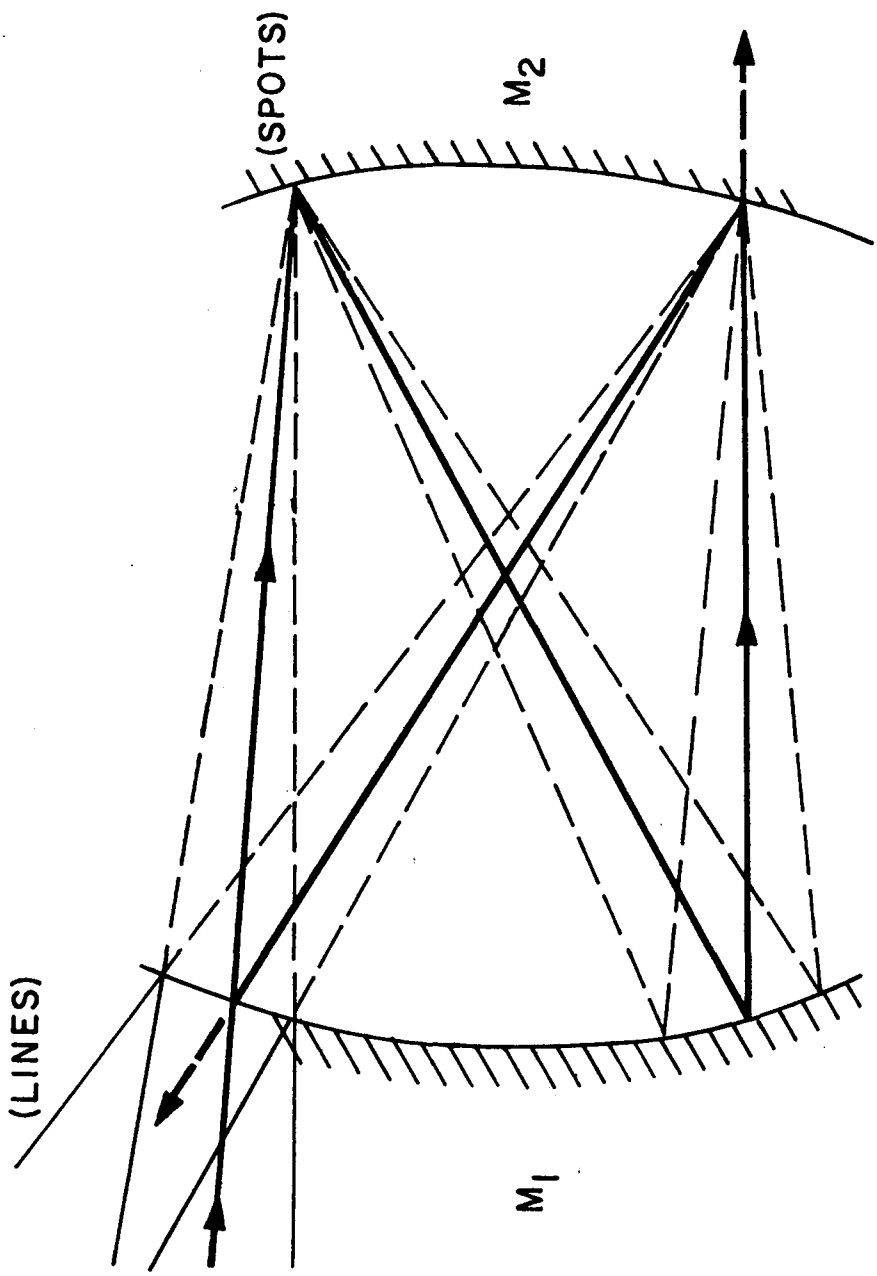

FIGURE A-1. INTERLACED MODE PATTERN OF OFF AXIS INTERFEROMETER

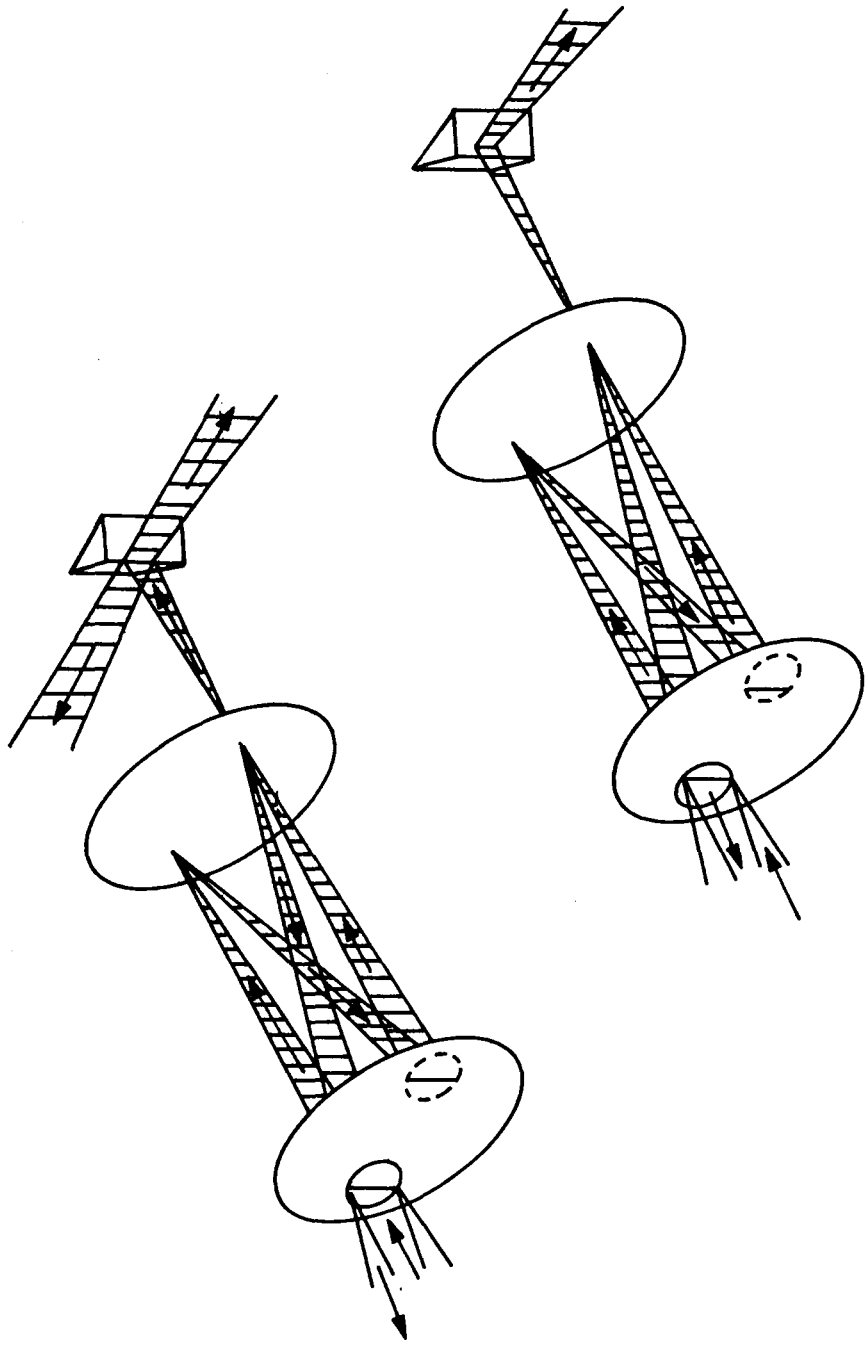

FIGURE A-2. BEAM ANGLE CHANGE IN OFF AXIS INTERFEROMETER

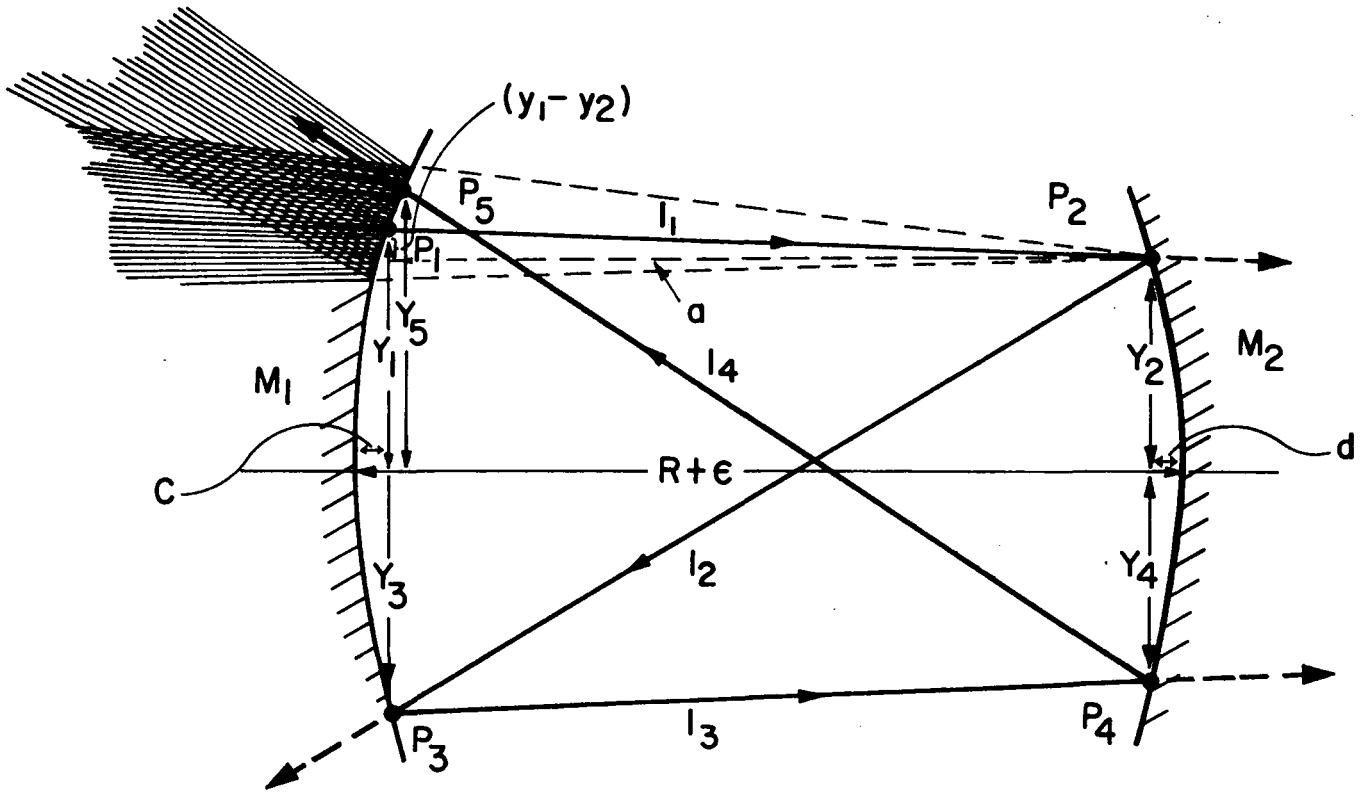

FIGURE A-3 RAY TRACING IN OFF AXIS INTERFEROMETER

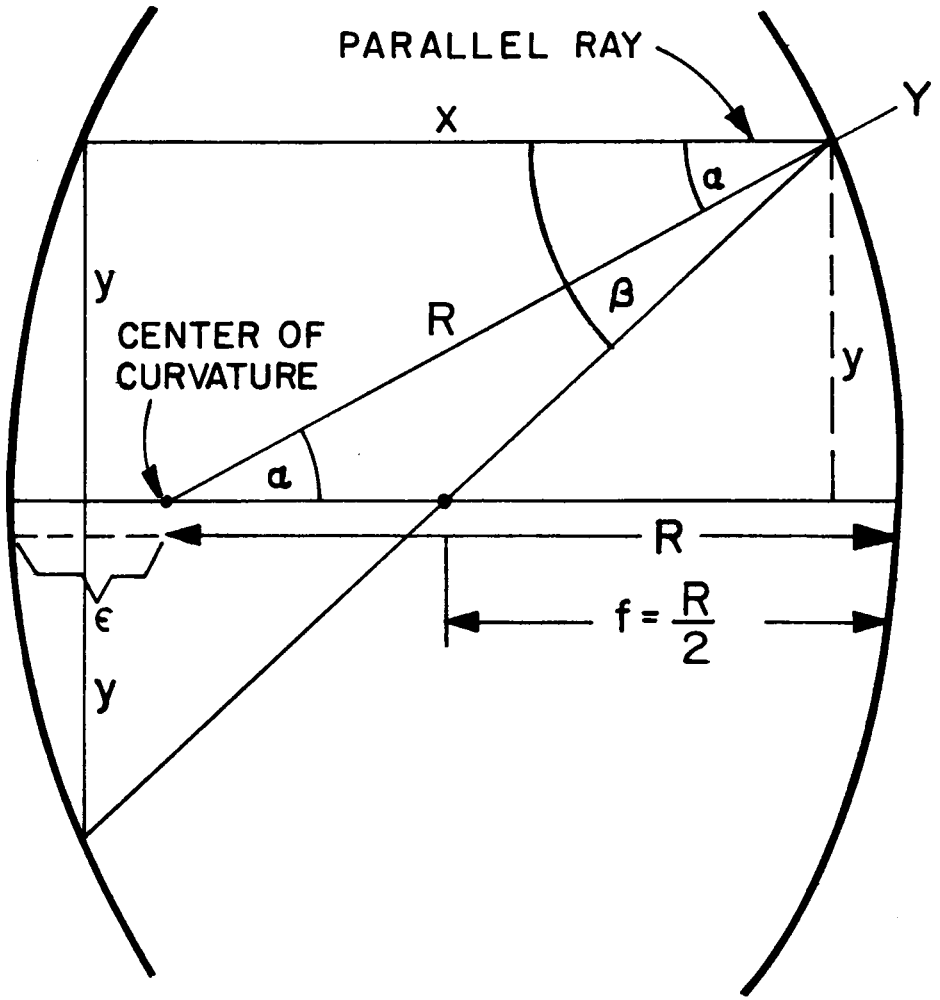

FIGURE A-4. REFLECTED RAYS

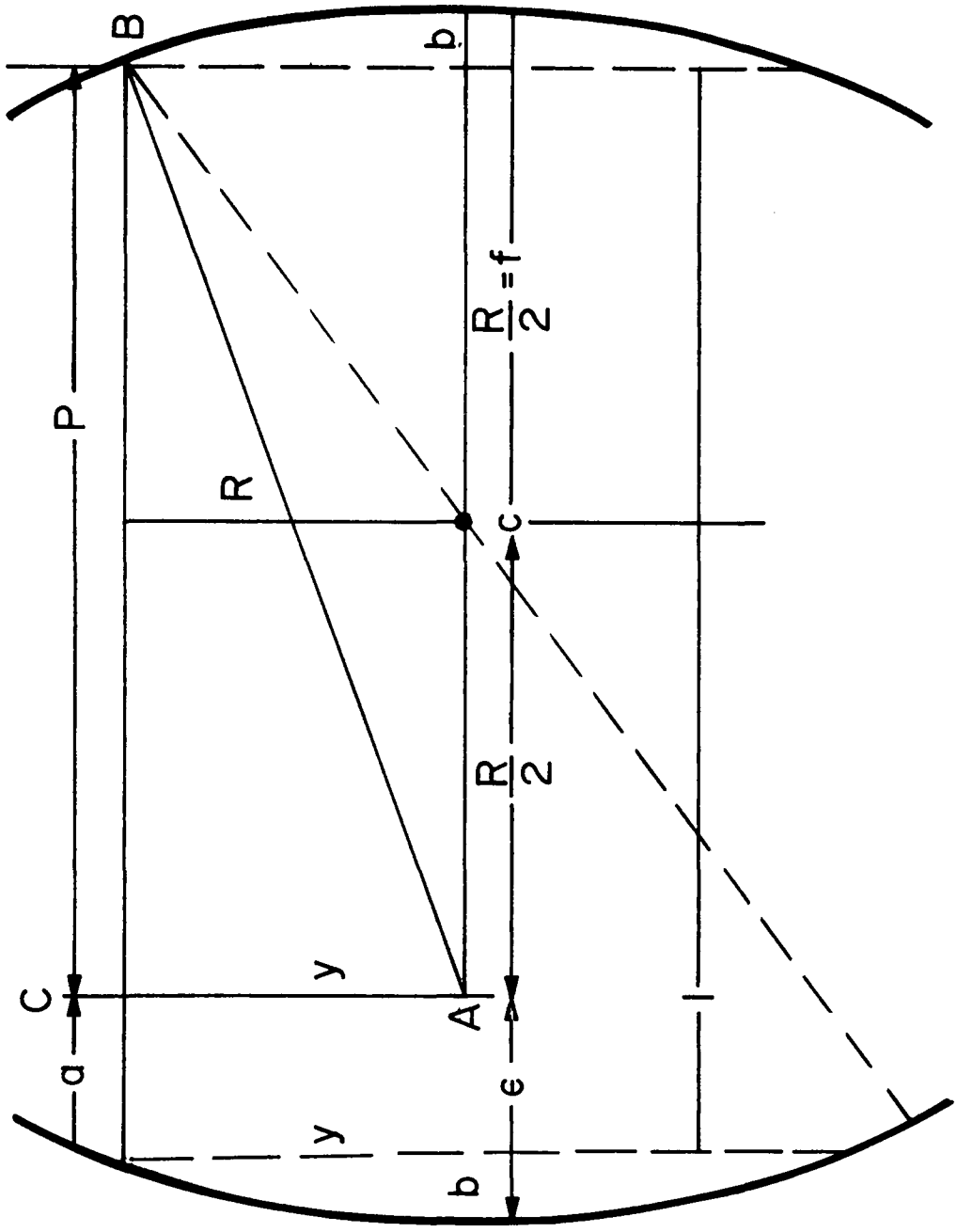

FIGURE A-5. CAVITY MIRROR SPACING

FREQUENCY STABILITY OF A HELIUM NEON LASER SYSTEM WITH EXTERNAL CAVITY CONTROL

By

Robert L. Kurtz

ABSTRACT

Many applications of gas lasers depend upon the extremely high spectral purity of their output signals. To fully exploit this remarkable spectral purity requires a high degree of frequency stabilization and laser mode control. In the past few years much effort has been expended in attempts to devise and test various methods of frequency stabilization. This investigation lists a number of these methods employed over the past few years. Further, it describes a state-of-the-art system employing two identical lasers and utilizing a combination of several of the known methods of frequency stabilization plus the use of an external cavity to passively control the frequency of the Fabry-Perot laser cavity. Data from this system has been analyzed and the state-of-the-art results of long term and short term relative frequency stability is presented.